# Putative Role of Connectivity in the Generation of Spontaneous Bursting Activity in an Excitatory Neuron Population

A Thesis
Presented to
The Academic Faculty

by

**Jie Shao**

In Partial Fulfillment
of the Requirements for the Degree
Master of Science in Bioengineering

Georgia Institute of Technology

July 2004

# Putative Role of Connectivity in the Generation of Spontaneous Bursting Activity in an Excitatory Neuron Population

Approved by:

Dr. Robert J. Butera, Advisor

Dr. Ronald L. Calabrese

Dr. Robert H. Lee

Date Approved: 8 July 2004

# TABLE OF CONTENTS

# LIST OF FIGURES

# ACKNOWLEDGEMENTS

I would like to thank Dr. Butera, my advisor, for giving me this very interesting research project and for providing me very good guidance on my thesis. I am impressed with his patience and his encouragement in the process of doing the project. I also would like to thank the other members of my thesis committee, Ronald Calabrese and Robert Lee, for their work to help me graduate.

I would especially like to thank my parents and my sister for their support during my study in USA. Their love and understanding are essential for me to go through the hard situations.

Finally, I would like to thank Edgar Brown for his very fruitful discussions with me during my thesis research.

# SUMMARY

Population-wide synchronized rhythmic bursts of electrical activity are present in a variety of neural circuits. The proposed general mechanisms for rhythmogenesis are often attributed to intrinsic and synaptic properties. For example, the recurrent excitation through excitatory synaptic connections determines burst initiation, and the slower kinetics of ionic currents or synaptic depression results in burst termination. In such theories, a slow recovery process is essential for the slow dynamics associated with bursting.

This thesis presents a new hypothesis that depends on the connectivity pattern among neurons rather than a slow kinetic process to achieve the network-wide bursting. The thesis begins with an introduction of bursts of electrical activity in a purely excitatory neural network and existing theories explaining this phenomenon. It then covers the small-world approach, which is applied to modify the network structure in the simulation, and the Morris-Lecar (ML) neuron model, which is used as the component cells in the network. Simulation results of the dependence of bursting activity on network connectivity, as well as the inherent network properties explaining this dependence are described. This work shows that the network-wide bursting activity emerges in the small-world network regime but not in the regular or random networks, and this small-world bursting primarily results from the uniform random distribution of long-range connections in the network, as well as the unique dynamics in the ML model. Both attributes foster progressive synchronization in firing activity throughout the network during a burst, and this synchronization may terminate a burst in the absence of an obvious slow recovery process. The thesis concludes with

possible future work.

# CHAPTER I

# INTRODUCTION

## *1.1 Population-wide Synchronized Bursting in Excitatory Neural Networks*

Spontaneous rhythmic activity is crucial for the formation and maturation of developing neural networks [26]. It is also widespread in the mature central nervous system, controlling repetitive rhythmic movements, such as, respiration and locomotion. One ubiquitous phenomenon found in a variety of neural circuits is population-wide synchronized rhythmic bursts of electrical activity. Examples include components of the respiratory rhythm generating circuitry in the brainstem [21], rhythms in the neonatal rat spinal cord [2] and developing neural networks in the retina of the immature ferret [11]. One class of such networks are those where the connectivity is predominantly mediated by excitatory chemical synapses. For example, in transverse brainstem slices, rhythmic bursting persists when inhibition is blocked and is reversibly eliminated by the blockade of excitatory synaptic transmission [21]. In the disinhibited embryonic rat and chick spinal cords, spontaneous bursts persist after inhibitory transmission is blocked [22, 16].

Excitatory neural networks that exhibit spontaneous population-wide bursting activity may consist of different types of synaptic connectivity and individual cellular properties. Proposed mechanisms explaining a regenerative process for burst initiation and a slower recovery process underlying burst termination are generally attributed to intrinsic and synaptic properties. For instance, based on the identification of voltage-dependent bursting pacemaker neurons in the pre-Bötzinger Complex

[21], rhythmic network bursting observed in the brainstem slices may result from excitatory coupled pacemaker neurons. In particular, burst initiation is attributed to the combination of intrinsic cellular properties and recurrent excitatory coupling, and burst termination is due to the slower kinetics of ionic currents intrinsic to the bursting neurons [17]. In the spinal cord of the chick embryo, where individual bursting neurons are not found, it is observed that the network excitability is depressed during the activity episode of a burst and recovers in the quiescent phase [8]. The depression mainly results from an activity-dependent decrease in synaptic strength. Thus for synchronized bursting in the disinhibited spinal cord, burst initiation is attributed to recurrent excitation and termination is attributed to the slower kinetics associated with synaptic depression [23].

In most discussions of mechanisms for rhythmic bursting, a recovery process with slower kinetics, whether it is intrinsic or synaptic, is responsible for the slower dynamics associated with bursting. However, recent experimental results [6] suggest that network bursts may occur when a presumed slow recovery process is blocked. In this experiment, the rhythmic bursting of pacemaker neurons in a transverse brainstem slice is abolished by applying riluzole, a blocker of the persistent sodium current, yet network bursts continue with the same oscillatory frequency. The slow inactivation of this current had previously been hypothesized to play a critical role as the slow process underlying bursting [3, 4, 5]. An alternative hypothesis that does not take into account a slow time-scale process may be considered to explain this generation of network bursts.

## *1.2 Small-world Networks*

Small-world phenomena are seen in everyday life. For example, while talking to a completely unknown stranger, it is realized that both of you share a common friend. This phenomenon has been expressed as "six degrees of separation" [9] by stating

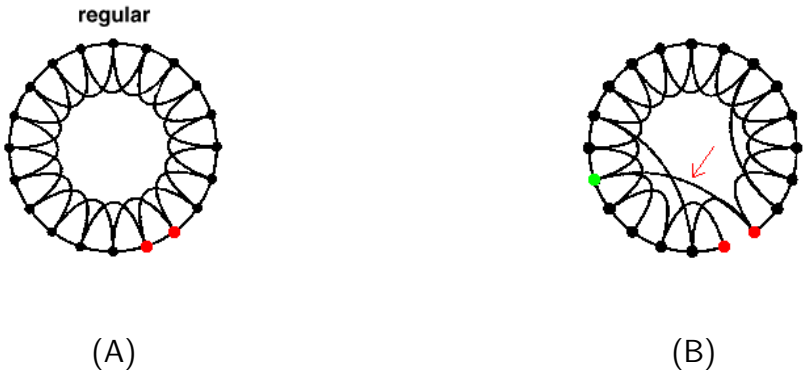


**Figure 1:** *The rewiring procedure.* (A) In a regular network, the edge between the two red nodes is chosen, with probability $p$, to be rewired. (B) The green node is randomly selected as the new target node. The local edge between the two red nodes is eliminated and a long connection between the red and green nodes, pointed by the red arrow, is established. With a predefined $p$, this process is performed on every edge in a regular network to create a new network structure.

that, on average, the number of intermediate persons between any two individuals on the planet is equal to or less than six. By utilizing a mathematical model, Watts and Strogatz proposed a novel network structure, the *small-world network*, to explain the small-world phenomenon. In their paper [24], they introduced a rewiring procedure to create a series of networks between the two extremes, regular and random networks. As shown in Figure 1, the rewiring procedure starts with a regular locally coupled network, with each node connecting to its $k$ nearest neighbors. Each edge in this network has a probability $p$ to be reconnected, that is, the probability for leaving the edge in place is $1 - p$ and probability for reconnecting the edge to another node, which is chosen uniformly at random over all nodes, is $p$.

As $p$ varies from 0 to 1, this approach creates a variety of networks with different connectivity architectures, as shown in Figure 2. $p = 0$ corresponds to a regular network, featured by a high density of local connections, since no edge is reconnected, and $p = 1$ corresponds to a random network, featured by a high density of distant edges, because each edge is reconnected to another node randomly chosen in the network. For intermediate values of $p$, the network is characterized by predominantly

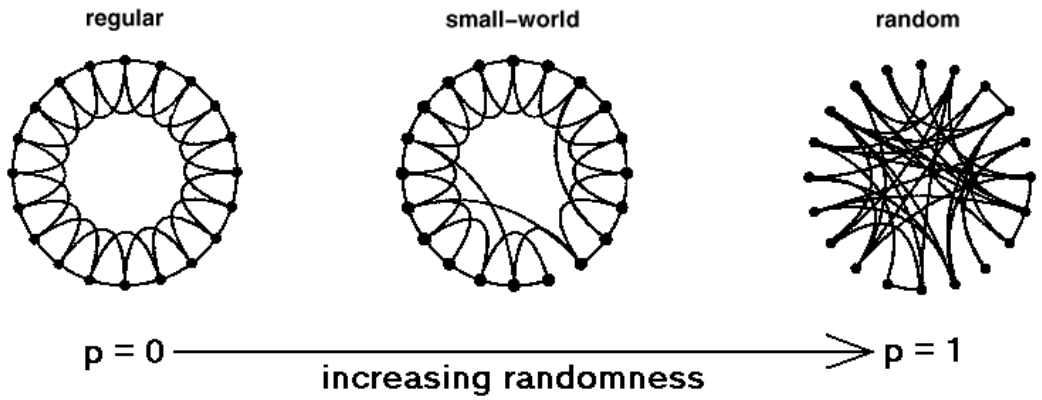


**Figure 2:** *A family of networks.* As the rewiring probability p increases from 0 to 1, a family of networks with different connectivity patterns are created. Especially, a network structure, the small-world network, presents between the two extremes, the regular and random networks.

local but a few long connections, a combination of features found in regular and random networks.

The characteristic path length $L$ and clustering coefficient $C$ are used to quantify the properties of network connectivity. As shown in Figure 3(A), $L$ measures the average separation between any pair of nodes. For any two vertices in the network, the shortest path between them is found and its length (i.e. number of "hops") is calculated. $L$ is the mean of all the shortest path lengths in the network. For an undirected graph with $N$ nodes,

$$L = \frac{\sum_{i=1}^{N-1}\sum_{j=i+1}^{N} L_{ij}}{\frac{N(N-1)}{2}}$$

$L_{ij}$ represents the number of "hops" in the shortest path between node i and node j.

As shown in Figure 3(B), $C$ measures the cliquishness of a neighborhood. For each vertex in the network, the number of edges that actually exists within a defined neighborhood is counted and divided by the maximum number of edges among the neighbors (in an undirected graph, the maximum number of edges within $k$ neighbors is $\frac{k(k-1)}{2}$). The fraction is defined as the clustering coefficient of each node. $C$ is the average of all the individual clustering coefficients in the network. For an undirected


**Figure 3:** *The illustration of calculating the characteristic path length L and clustering coefficient C.* (A) The shortest path between a pair of nodes (the two red nodes). Among all the possible paths between the two red nodes, the one that uses the green node as the intermediate is the shortest path (the one that passes the orange nodes is a valid but not the shortest path). The length of the path is defined as the number of "hops", rather than the summation of the actual length of each edge on the route. $L$ is the average of the shortest path lengths between each pair of nodes in the network. (B) The clustering coefficient of a node (the red node). The red node has 4 neighbors marked as green nodes. In an undirected graph, the maximum number of edges that could exist among 4 nodes is 6 while the number of the edges that actually appears among these 4 neighbors is 1 (the edge pointed by the red arrow). The clustering coefficient for the red node is defined as 1/6. $C$ is the mean of the clustering coefficient for each node in the network.

graph, if node i has $k_i$ neighbors

$$C = \frac{1}{N}\sum_{i=1}^{N}\frac{C_i}{\frac{k_i(k_i-1)}{2}}$$

$C_i$ represents the number of connections existing among the $k$ neighbors of node $i$.

Figure 4 shows that, in terms of these two measures, a regular network has large $C$ and $L$, a random network has small $C$ and $L$, while a small-world network has large $C$ but small $L$, featured by a heavily clustered local neighborhood and a small average distance between nodes.

The small number of long connections is responsible for large $C$ and small $L$ in a small-world network. The removal of a few local edges from their neighborhood only slightly reduces $C$. On the other hand, a few long connections, resulting from the reconnection of the local edges, significantly shorten the distance not only between the two directly connected nodes but also between their immediate neighbors, as well

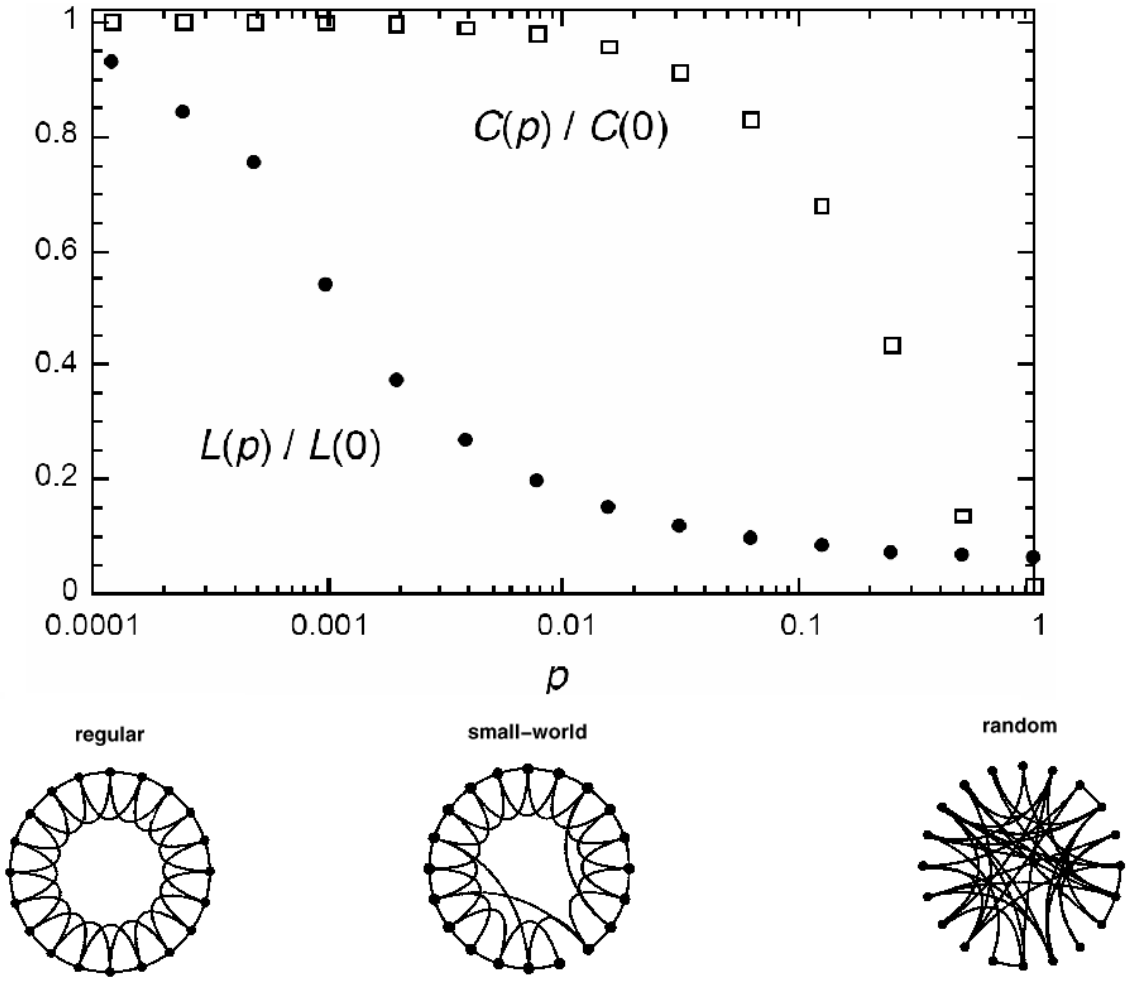


**Figure 4:** *The two measures $C$ and $L$ on the regular, small-world and random networks.* For each $p$, a network is constructed from the regular network by the rewiring procedure. Then $C$ and $L$ for this new network are calculated. So the network structure and consequently $C$ and $L$ are a function of $p$. As $p$ increases from 0 to 1, a series of networks are created and $C$ and $L$ are computed for each network ($C(p)$ and $L(p)$). Then $C(p)$ and $L(p)$ are normalized by $C(0)$ and $L(0)$, $C$ and $L$ of the regular network, respectively. The normalized curves, $C(p)/C(0)$ and $L(p)/L(0)$, show that the regular network ($p = 0$) has large $C$ and $L$, the random network ($p = 1$) has small $C$ and $L$, while a small-world network ($0 < p < 1$) has $C$ being almost as large as the one in the regular network, and $L$ being nearly as small as the one in the random network [24].

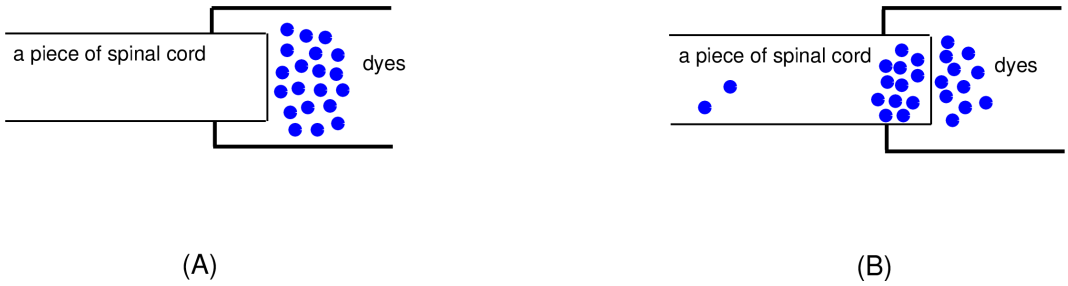


**Figure 5:** *An illustration of the experiment which reveals that the neural network in the spinal cord may share the feature of a small-world network.* (A) A piece of spinal cord immersed in the dye solution. The dyes, indicated by the blue dots, would stain the nuclei of cells when they are taken up by the neurons. (B) After certain time, the dyes enter the neurons by endocytosis and color the nuclei. Most neurons marked by the dyes are located in a small region which contacts with the dye solution. However, a few distant neurons are also marked because their axons project to the small region. So in this network, many neurons are highly clustered in a local region while they also receive inputs from a few remote neurons. This connectivity pattern is shared by the small-world network [25].

as their indirect neighbors, which leads to the steep decrease in $L$. Due to these few long connections, although we live in small groups in different local regions, spreading over the world, on average, we are only six degrees of separation away from anybody else on the earth.

Besides clearly explaining the small-world phenomenon, the small-world network paradigm may have a variety of applications. One potential application is as a connectivity model of neural networks. For example, Watts and Strogatz examined the simple neural network of the worm, *Caenorhabditis elegans* [24], in which the connections between each pair of neurons have been mapped out. They found that compared to a random network with the same number of neurons and average number of connections per neuron, this network has large $C$ and small $L$, the characteristic of a small-world network. Furthermore, as illustrated in Figure 5, the experiments on the neural network in the spinal cord show that in a small region, neurons are predominantly locally connected and a few remote neurons have long projections to this region. This connectivity pattern is shared by a small-world network.

The utility of the rewiring procedure in creating a family of networks with different connectivity properties and the indication that biological neural networks may have the small-world network structure prompt us to use the small-world approach in our simulation to investigate the effect of connectivity patterns on the network-wide bursting activity.

## *1.3 Morris-Lecar Neuron Model*

The model of Morris and Lecar (ML) [15] was originally developed to characterize the electrical activity of the barnacle muscle fiber. The model consists of three ionic currents: a calcium current, a potassium current and a leak current. The inward calcium current activates instantaneously, which makes it only a function of voltage, and it does not possess inactivation. The following equations describe the kinetics of this current.

$$\begin{aligned} I_{Ca} &= \bar{g}_{Ca} m_\infty(V)(V - E_{Ca}) \\ m_\infty(V) &= 0.5(1 + tanh(\frac{V - V_1}{V_2})) \end{aligned}$$

The outward potassium current is an active current with activation depending on both voltage and time, and it does not have inactivation. This current is modeled by the following equations.

$$\begin{aligned} I_K &= \bar{g}_K w(V - E_K) \\ \frac{dw}{dt} &= \phi \frac{w_\infty(V) - w}{\tau_w(V)} \\ w_\infty(V) &= 0.5(1 + tanh(\frac{V - V_3}{V_4})) \\ \tau_w(V) &= \frac{1}{cosh(\frac{V - V_3}{2V_4})} \end{aligned}$$

The leak current is a passive current, which is a function of voltage. And it is described by the equation below.

$$I_L = \bar{g}_L(V - E_L)$$

The change of the membrane voltage is determined by the above ionic currents and the capacitance of the cell membrane, and is described by the following equation.

$$C\frac{dV}{dt} = -\bar{g}_{Ca}m_{\infty}(V)(V - E_{Ca}) - \bar{g}_K w(V - E_K) - \bar{g}_L(V - E_L)$$

The ML equations and the meanings of the parameters are described in detail in Appendix A.

As a conductance-based, two-dimensional neuron model, the ML equations possess the general characteristics of excitation and recovery underlying an action potential and thus are viewed as a prototypical neural oscillator, as shown in Figure 6. Compared to the four-dimensional Hodgkin-Huxley (HH) neuron model, the ML equations have much simpler dynamics and have been applied to describing the dynamics of various biological neurons. For example, the ML equations have modeled pacing activity in rabbit sinoatrial myocytes [7]; coincidence detection in bipolar neurons in the mammalian auditory brainstem [1]; local interneurons underlying patterned rhythms in the swimmeret of crayfish [20]; and clustered and synchronized electrical activity among hippocampal CA3 neurons [14].

In addition, under different parameter regimes, ML dynamics are qualitatively distinct in terms of their phase-plane trajectories and phase-response characteristics, that is, the ML model is capable of exhibiting either class I or class II excitability [18]. As shown in Figure 7, with the increase in the amplitude of applied depolarizing current, a silent neuron begins to fire with a gradual increment in firing rate. A neuron shows class I excitability if its lowest firing frequency is close to zero and the transition from silent to oscillatory state occurs via a saddle-node bifurcation. Class II excitability exists if the lowest firing frequency is a non-zero positive value and the transition from silent to oscillatory state occurs via a Hopf bifurcation.

Because of its dynamical simplicity, ability to generate intrinsic oscillations through multiple bifurcation mechanisms [18], and its utility in modeling the general characteristics of neural oscillations [10], whether those oscillators are spiking or bursting

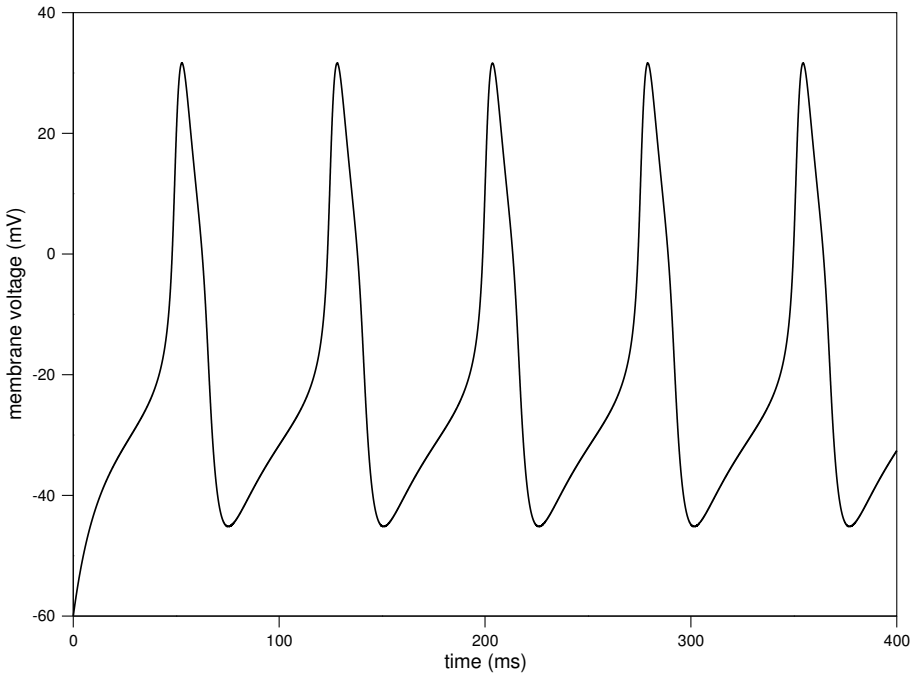


**Figure 6:** *The action potential generated by the Morris-Lecar equations.*After injected a constant current of 2.5 $\mu A/cm^2$, a Morris-Lecar model neuron is depolarized from the resting membrane potential of $-60$ mV and generates a train of action potential with the oscillatory frequency of 13.4 Hz.

neurons [19], the ML neuron model was chosen as the component cells in the network.

## *1.4 A Prelude of Things to Come*

In this thesis, a new mechanism has been explored for achieving network-wide synchronized bursting in excitatory networks, which does not rely on the existence of a slow kinetic process on the order of the time scale of bursting. Rather, the mechanism for bursting is dependent on specific patterns of connectivity among the component neurons. The model network is composed of ML neurons and its connectivity is systematically varied by the small-world paradigm. The thesis describes the selection of network structure, the essential properties of the input response of the ML model, and "Cellular Automaton"(CA) model, which captures the essential features of the ML dynamics. The simulation results show that network bursts emerge when the

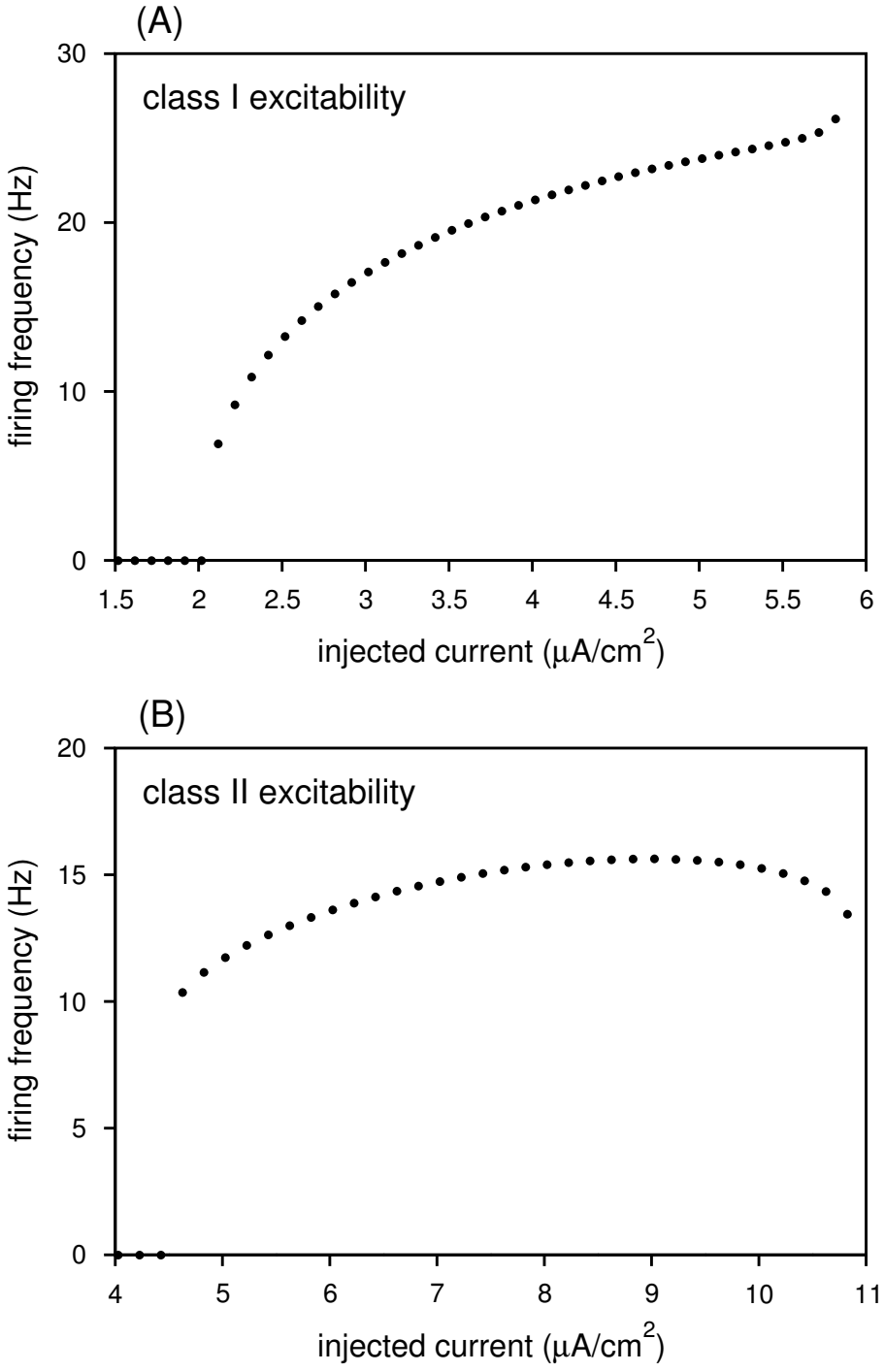


**Figure 7:** *The class I and class II excitability of a Morris-Lecar neuron.* As the injected current increases, a silent neuron begins to fire with an increment of the oscillatory frequency. In the transition from silent to firing state, the lowest firing frequency can be either (A) arbitrarily close to zero, called class I excitability, or (B) above a certain value, called class II excitability.

ML model neurons are coupled in a small-world connectivity pattern. The robustness of this small-world bursting is tested under a range of network parameters for randomly generated parameter sets. The thesis then presents the exploration of mechanisms that support small-world bursting and reveals that both the distribution of long connections in a small-world network and ML dynamics play important roles in synchronizing the firing activity across the entire population. Synchronization might be the mechanism for burst termination in the absence of a slow recovery process. The thesis concludes with a discussion of possible future work.

# CHAPTER II

# METHODS

## *2.1 Structure of the Neural Network*

In the small-world approach, proposed by Watts and Strogatz [24], a rewiring procedure is applied to construct a family of networks including regular, small-world and random networks. The two static measures of network connectivity, the characteristic path length $L$ and clustering coefficient $C$, are calculated and small-world networks are shown to exhibit large $C$ and small $L$. The small-world region, in which $C$ is large and $L$ is small, is almost independent of the changes of $k$ (the neighborhood size). However, this region is significantly enlarged by the increase of $N$ (the number of nodes in the network), as shown in Figure 8.

Meanwhile, with large $N$, the increase of the small-world region becomes less obvious but the computational time is consumed dramatically. As a trade-off between a distinguished small-world region and reasonable computational time for network simulations, a network with $N = 512$ and $k = 10$ was chosen in the simulation. The static property of the network and the qualitative division of regular, small-world and random network regimes are shown in Figure 9.

The network consists of 512 neurons, forming a ring with neuron #0 next to neuron #511. Neuron #0 and its 10 neighbor neurons, located at a small local region of the network, are referred to as the pacing neurons and fire repetitively, while the other neurons remain at rest in the absence of synaptic inputs.

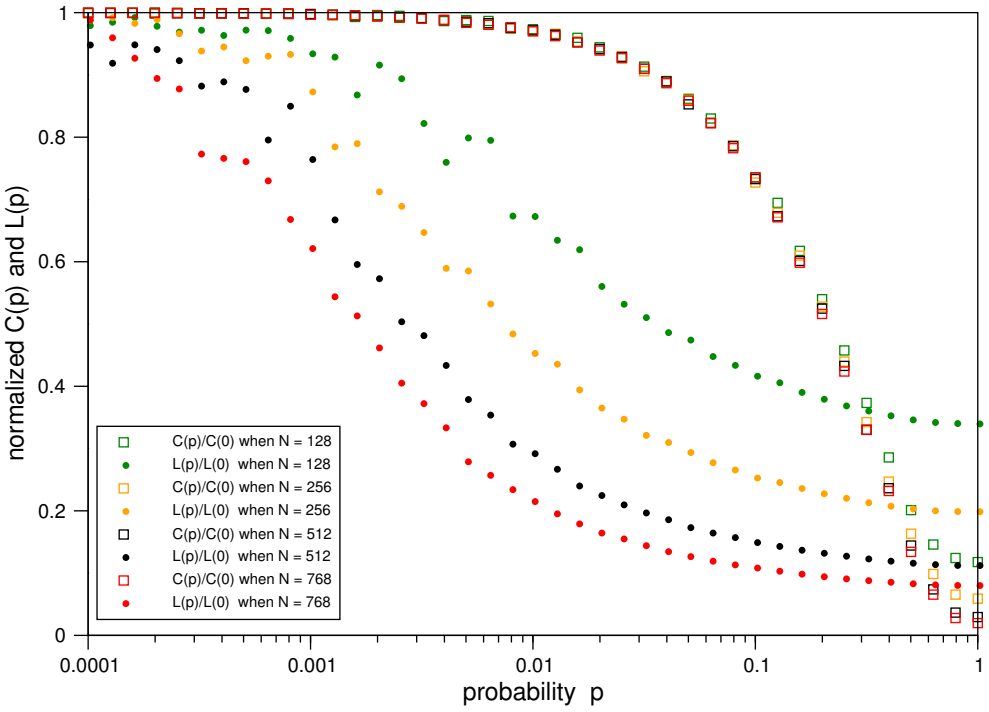


**Figure 8:** *The small-world region is significantly affected by the increase of N.* The normalized clustering coefficient $C(p)$ and characteristic path length $L(p)$ are plotted when $N$, the number of nodes in the network, is $128, 256, 512$ and $768$, respectively. As $N$ increases, the $C(p)/C(0)$ curve almost does not change but the $L(p)/L(0)$ curve drops. So the small-world region with large C and small L is enlarged by the increment in N. However, the drop of $L$ is nonlinear with the increase of $N$. When $N$ changes from 128 to 256 or from 256 to 512, the decrease of $L$ is obvious but the further increase of $N$ from 512 to 768 results in neither a distinct drop of L nor a significant increase in the small-world region.

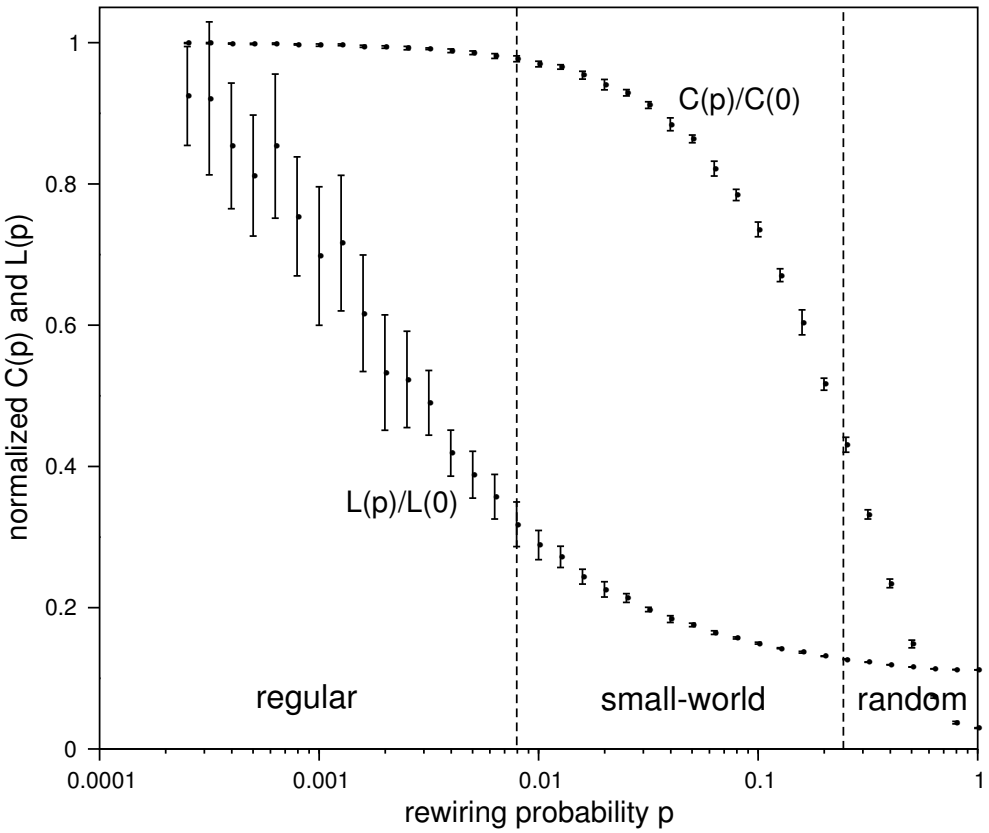


**Figure 9:** *The normalized characteristic path length $L(p)$ and clustering coefficient $C(p)$ in the network with $N = 512$ and $k = 10$.* The results are averaged over 10 random rewiring procedures for constructing networks (the error bars show the standard deviation of the 10 random cases) and normalized by $L(0)$ and $C(0)$ of the regular network. The qualitative division of regular, small-world and random regimes is illustrated by the two vertical dashed lines.

## 2.2 The Input Response of the Morris-Lecar Neuron Model

The ML model is distinct from a canonical neuron model, such as the Hodgkin-Huxley (HH) or integrate-and-fire (IF) model, in its response to the two successive transient current pulses. An action potential developed by a canonical model has a well-defined absolute and relative refractory period. On the contrary, due to the lack of inactivation, the ML model has no absolute refractory effect, and can respond to an input at any phase during excitation and repolarization. In particular, as shown in Figure 10, if the membrane potential is higher than the threshold when the second input arrives, the time the voltage spends above the threshold is extended, that is, the repolarization of the action potential is delayed (as shown in Figure 10(B), (D)). However, if the membrane potential is below threshold but above rest when the cell receives the second input, a threshold-crossing event is triggered. This occurs even if the amplitude of the second input is significantly smaller than that of the first input (as shown in Figure 10(C)). Such dynamics are more akin to the properties of bursting instead of spiking neurons, and consistent with the notion of the ML model as characterizing an envelope of bursting activity.

## 2.3 Cellular Automaton Model

A cellular automaton (CA) model was developed to capture the input/output dynamics of the ML model in as simple form as possible, similar to using the IF model to characterize action potentials. The detailed description of CA model is listed in Appendix B.

In a CA, each cell stays at one of a finite number of states. Depending on the current states of the cell and its neighbors, the cell state in the next time step is determined. The states of all cells in the entire population are updated simultaneously and advance in discrete time steps.

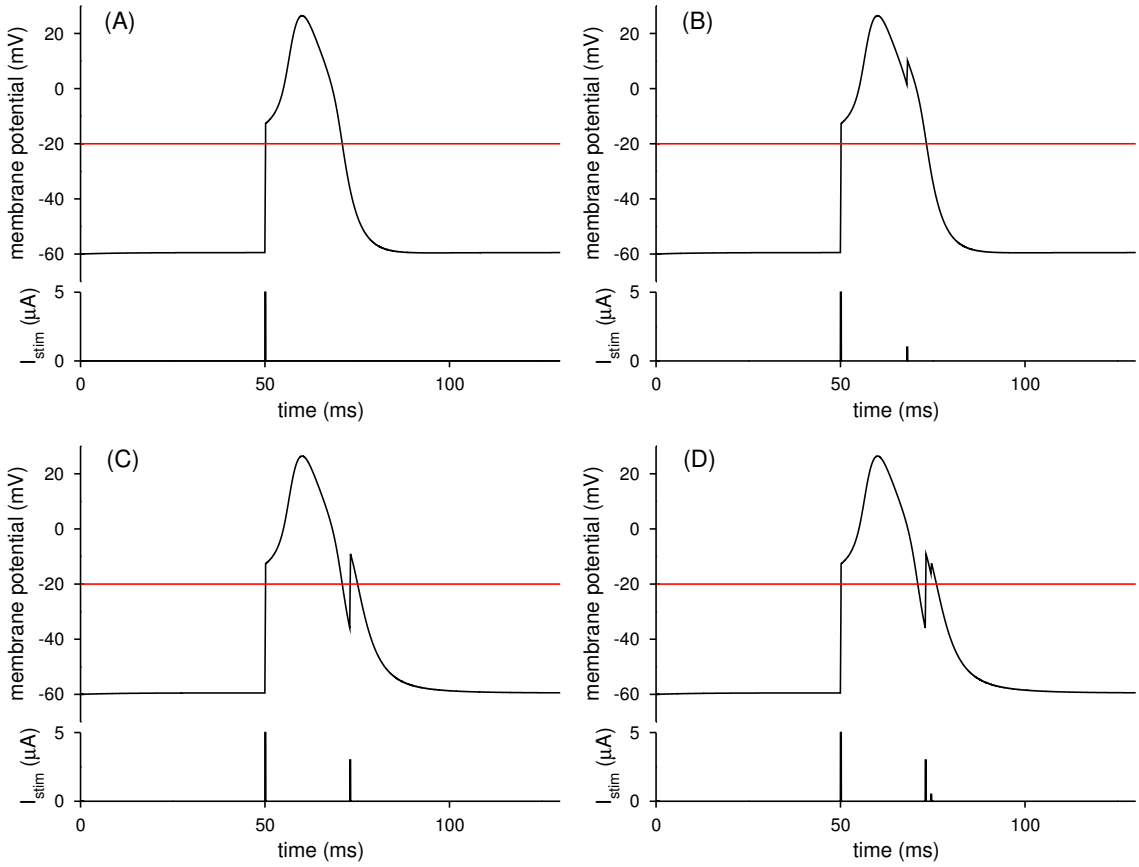


**Figure 10:** *The response of Morris-Lecar model to successive transient current impulses.* (A) A current impulse at 50 ms with amplitude 5 $\mu A$ and duration 0.2 ms triggers an action potential. (B) After the first current impulse at 50 ms generates an action potential, the second current impulse with amplitude 1 $\mu A$ and duration 0.2 ms occurs at 68 ms. When the second impulse arrives, the membrane potential is higher than the threshold $-20$ mV. The second input causes an extension in the superthreshold duration of the action potential. (C) After the first current impulse at 50 ms generates an action potential, the second current impulse with amplitude 3 $\mu A$ and duration 0.2 ms occurs at 73 ms. When the second current impulse arrives, the membrane potential is lower than the threshold $-20$ mV but higher than the resting potential $-60$ mV. The second input causes a threshold-crossing event. (D) After the first input at 50 ms generates an action potential and the second input at 73 ms triggers a threshold-crossing event, the third current impulse at 74.5 ms with amplitude 0.5 $\mu A$ and duration 0.2 ms causes an extension in the superthreshold duration of the threshold-crossing event. The threshold of $-20$ mV is indicated by the red line.

In the CA model, each neuron stays at one of three states, that is, subthreshold, firing and superthreshold states. The state of a neuron is updated according to its current state and the states of other neurons which provide synaptic inputs to it. At every time step, each neuron in the network is calculated to determine its state in the next step. Three state variables $F, V, R$ with each being a $N \times 1$ vector are used in the CA model. Every element in the vectors, $F, V, R$, corresponds to each neuron in the network. The binary variable $F$ represents the transient firing state of neurons which just lasts for one step. $F_i = 1$ indicates neuron $i$ fires, otherwise, $F_i = 0$. The continuous variable $V$ represents the subthreshold state of neurons which decays with the rate $k$ at every cycle and element $V_i$ increases instantaneously by the number of synaptic inputs received by the subthreshold neuron $i$. If $V_i$ passes the firing threshold $M$, neuron $i$ enters the firing state, otherwise, it remains in the subthreshold state. The integer variable $R$ represents the superthreshold state of neurons which decreases by 1 at every step and element $R_i$ increases by $\Delta R$ when the superthreshold neuron $i$ receives any input. $R_i > 0$ indicates neuron $i$ is in the superthreshold state while $R_i = 0$ represents it is out of the superthreshold state. That the duration of the superthreshold state is extended by $\Delta R$ whenever an input is received by a superthreshold neuron simulates the properties of ML model shown in Figure 10(B)(D). The subthreshold state decays from $M$ when neuron $i$ is just out of the superthreshold state so $V_i$, with a small amount of additional input, can pass $M$ and neuron $i$ enters the firing state. This rule for updating state corresponds to a threshold-crossing event elicited by a small input in the repolarization phase of the ML action potential, as shown in Figure 10(C).

This discrete CA model greatly simplifies the computation since it only involves the matrix multiplication and a set of rules to change cell states, rather than solving coupled differential equations. Moreover, it discerns the main characteristics in ML model that support network-wide bursting activity when connectivity patterns fall in

the small-world regime.

# CHAPTER III

# RESULTS

## *3.1 Network-wide Bursting Activity in the Small-world Regime*

The component cells in the network are ML-type neurons with class I excitability (the parameter set of a ML neuron exhibiting class I excitability is listed in Appendix A). Under a constant applied current of 2.5 $\mu A/cm^2$, the pacing neurons fire with a frequency of 13.4 Hz. The resting neurons are stimulated with a small current randomly assigned from a normal distribution with zero mean and a standard deviation of 0.66 $\mu A/cm^2$ and thus have a depolarized or hyperpolarized subthreshold potential. The initial membrane voltage of all neurons is set to $-60$ mV. The synaptic properties are determined by a synaptic strength of 0.01 $\mu S$ and a synaptic delay of 1.5 ms (both the synaptic strength and delay are the same for each synaptic connection). By implementing the network in the simulation package NEURON [12, 13] and allowing the transients to die out, we observed that in this purely excitatory network, firing activity patterns change dramatically as the connectivity topology transits through regular, small-world and random regimes, as shown in Figure 11.

In the regular regime (Figure 11(A)), the excitation originates from the pacing neurons at the top of the ring, propagates to other silent neurons along the left and right halves of the ring, and eventually ends on the other end of the ring. This propagation pattern recurs with 13.4 Hz frequency, the same as the firing rate of the pacing neurons. In the small-world regime (Figure 11(B)(C)), with the presence of a few long connections, bursting activity, characterized by alternative episodes of firing and quiescence, appears. In Figure 11(B), a burst starts with an approximately

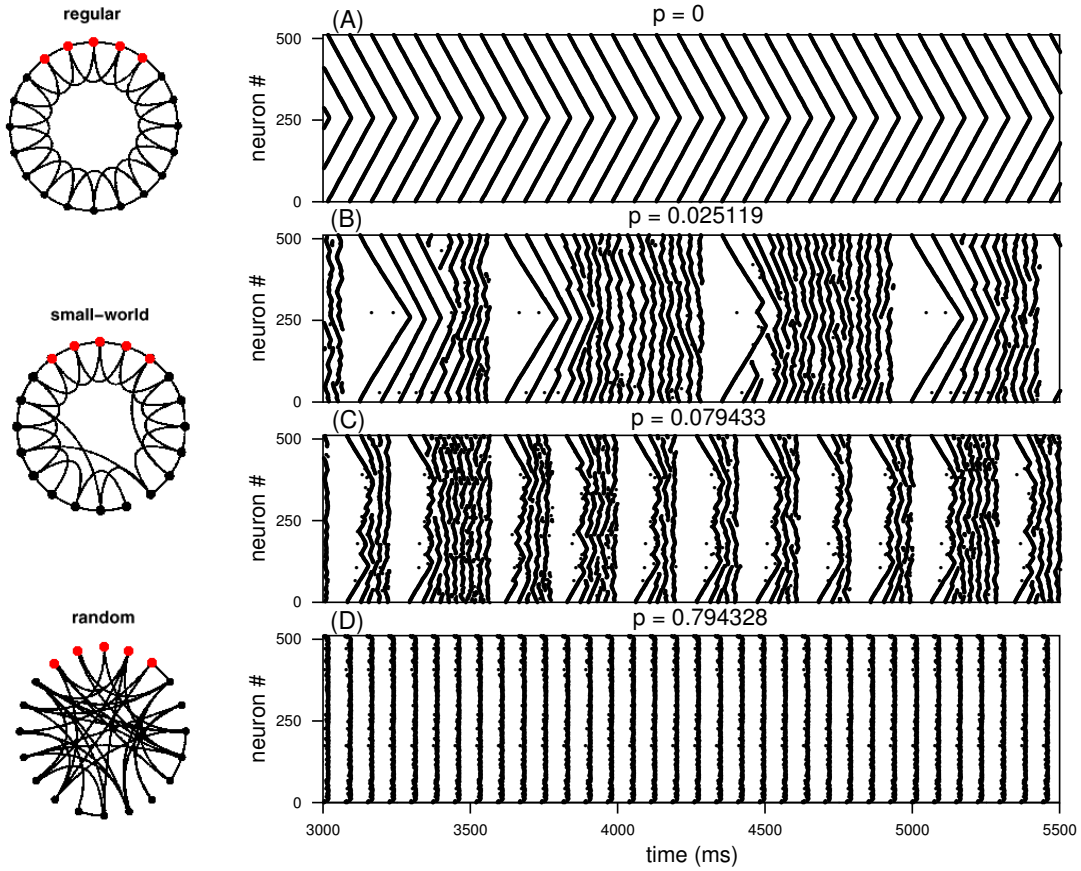


**Figure 11:** *Raster plots of firing activity in regular, small-world and random network regimes.* In the left column, the first ring illustrates the structure of a regular network, and (A) shows the firing activity in the regular network regime. The second ring illustrates the structure of a small-world network, and (B) and (C) show the firing activity in the small-world network regime. The third ring illustrates the structure of a random network, and (D) shows the firing activity in the random network regime. The neurons marked red on the rings show the pacing neurons. The networks that generate the firing activity shown in the raster plots share the same structural features of the three rings but with a much larger scale. They have 512 neurons with each neuron having 10 neighbors, and are driven by 11 pacing neurons located on the top of the ring.

orderly propagation wave but the duration of each "wave" progressively decreases as the burst develops. When all neurons in the network fire almost synchronously, a burst terminates and the network remains silent until the pacing neurons initiate the next burst. In Figure 11(C), with the increase of long connections, the development of the synchronized firing activity throughout the network becomes faster and thus the burst occurs at higher frequency with narrower duration. In the random regime (Figure 11(D)), the large number of long connections with short mean path length causes the nearly synchronized spiking activity at the same frequency as that of the pacing neurons (13.4 Hz).

To quantitatively demonstrate the emergence of bursting activity in small-world networks, we computed the dominant frequency of rhythmic network activity for different connectivity patterns. On the raster plot of network activity, we calculated the histogram of spike times with bin size 20 ms, as shown in Figure 12(A), then we performed a Fourier transform on the histogram and found the dominant frequency, the frequency component that has the highest amplitude in the frequency spectrum, as shown in Figure 12(B).

As shown in Figure 13, in the regular and random regimes, the dominant frequency is the same as the firing rate of the pacing neurons, representing the repeated network propagation and spiking activity, respectively. But in the small-world regime, the dominant frequency rapidly drops to a low value, corresponding to the slow bursting activity. Within the small-world regime, the bursting frequency increases with the rewiring probability $p$.

## *3.2 The Dependence of Network-wide Bursting Activity on Synaptic Delays*

To examine the effect of synaptic delays on network bursts in the small-world regime, we set the delay to five different values, that is, $0, 0.75, 1.5, 2.25$ and 3.0 ms. Typical

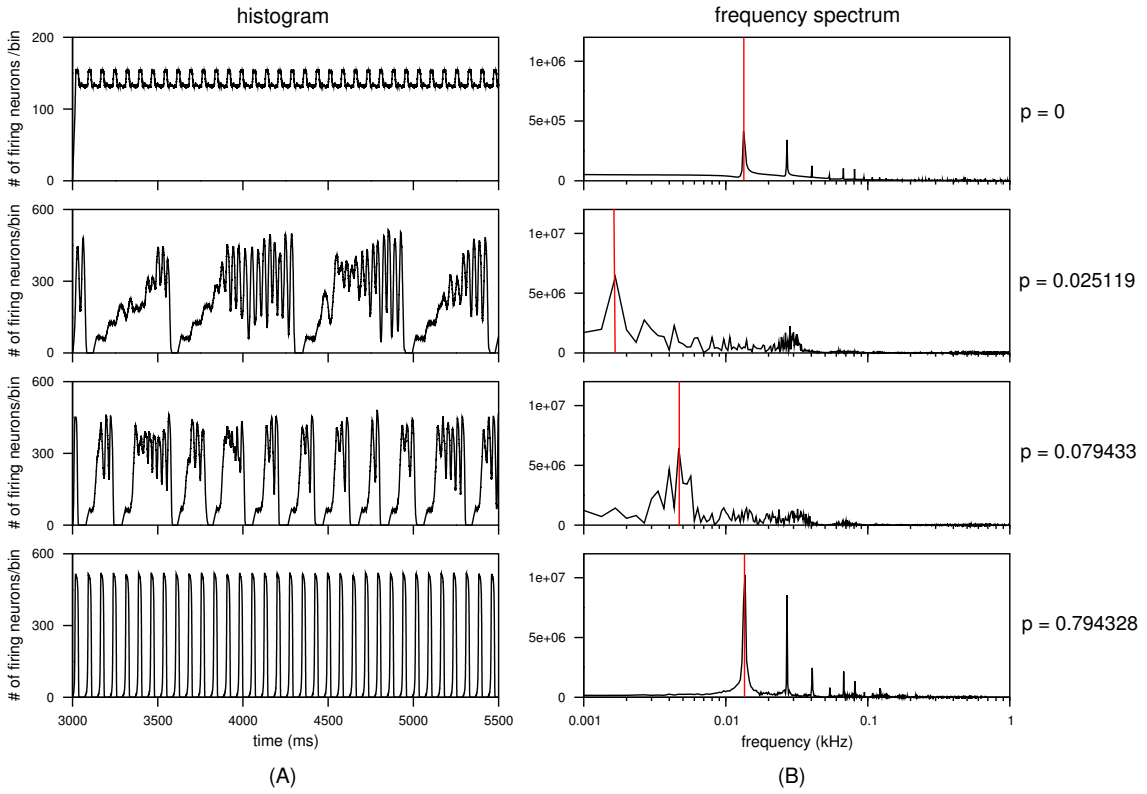


**Figure 12:** *Dominant frequencies of network activity shown in Figure 11* (A) Histogram of the network activity with the time bin size 20 ms. (B) Frequency spectrum of the histogram. The red line marks the dominant frequency, the frequency component which has the highest amplitude in the frequency spectrum.

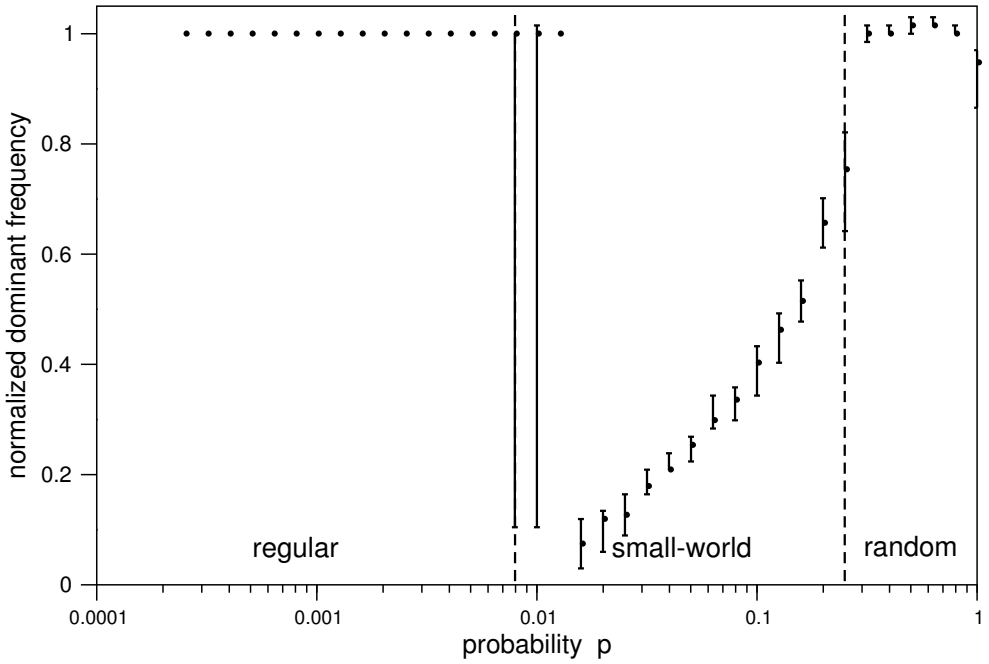


**Figure 13:** *Dominant frequency of the network activity.* As $p$ increases from 0 to 1, the approach illustrated in Figure 12 is used to find the dominant frequency of the firing activity in each network. The results are the medians of 40 random cases, 10 random rewiring procedures for each of the four initial conditions (the error bars represent the interquartile range of the 40 random cases) and normalized by the frequency of activity in the regular network (13.4 Hz).

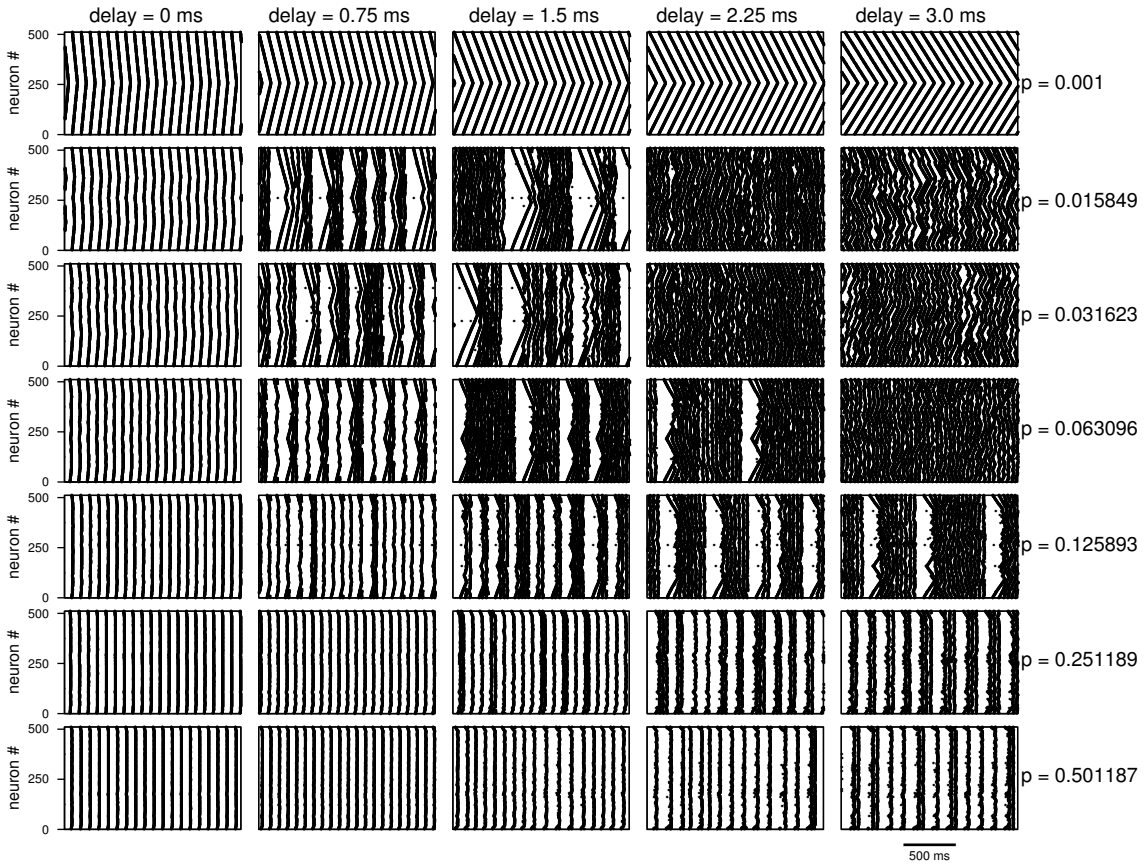


**Figure 14:** *Raster plots of network activity varying the synaptic delay.* Delay = $0, 0.75, 1.5, 2.25$ and 3.0 ms, respectively. The connectivity topology covers regular, small-world and random network regimes, as indicated by the rewiring probability $p$.

simulation results, as $p$ and synaptic delays are varied, are shown in Figure 14. When the delay is 0, no bursting activity appears for any value of $p$, whereas bursting activity exists in small-world regime when the delay is 0.75 or 1.5 ms. The network activity evolves to highly synchronized oscillations with shorter burst duration and period as the number of long paths increases. As the synaptic delay increases to 2.25 or 3.0 ms, the network dynamics converge to a self-sustained hyperexcited state, bursting with longer duration or synchronous spiking with occasional population-wide doublets. Therefore, this model shows that an appropriate delay plays a significant role on the emergence and parameter robustness of network bursting in the small-world regime.

## 3.3 The Parameter Robustness of Small-world Bursting

With a given set of parameters for neuron properties (class I excitability, $-60$ mV initial membrane potential and depolarized or hyperpolarized subthreshold resting voltage) and the number of connections in the network ($N = 512, k = 10$), bursting activity emerges in the small-world regime but not in regular or random networks. To investigate whether or not small-world bursting persists if the parameters are changed, we systematically varied specific parameters from their nominal values.

During variations in neuron excitability (class I or class II excitability) or neighborhood size $k$, the network bursts continued in small-world regime but with a significantly narrower range of $p$ for the appearance of bursts. As described in section 3.1, the normalized dominant frequency of network activity with a value significantly lower than 1 corresponds to the bursting activity. Figure 15(A) shows that under the default setting (class I excitability and $k$=10), bursting appears in a broad range of $p$. When the component ML cells have class II excitability (the parameter set for the neuron to possess class II excitability is listed in Appendix A), bursting activity mostly appears in the higher $p$ range of the small-world regime, as shown in Figure 15(B), while the lower $p$ end shows the hyperexcited activity. When the neighborhood size is doubled ($k = 20$), bursting develops at lower $p$ end of the small-world regime, as shown in Figure 15(C).

Due to the possibility of multiple coexisting states in an excitatory network, every simulation was rerun for multiple initial conditions. Changes in the initial conditions are realized by setting the initial membrane voltage to $-30$ mV, 0 mV (with the other state variable $w = w_\infty(V)$) or an uniform random distribution in $[-70, 10]$ mV with $w$ uniformly randomly distributed in [0,1]. Compared with control results from the default $-60$ mV initial membrane potential, the three distinct new initial conditions do not cause appreciable difference in the bursting activity. The neurons at rest are

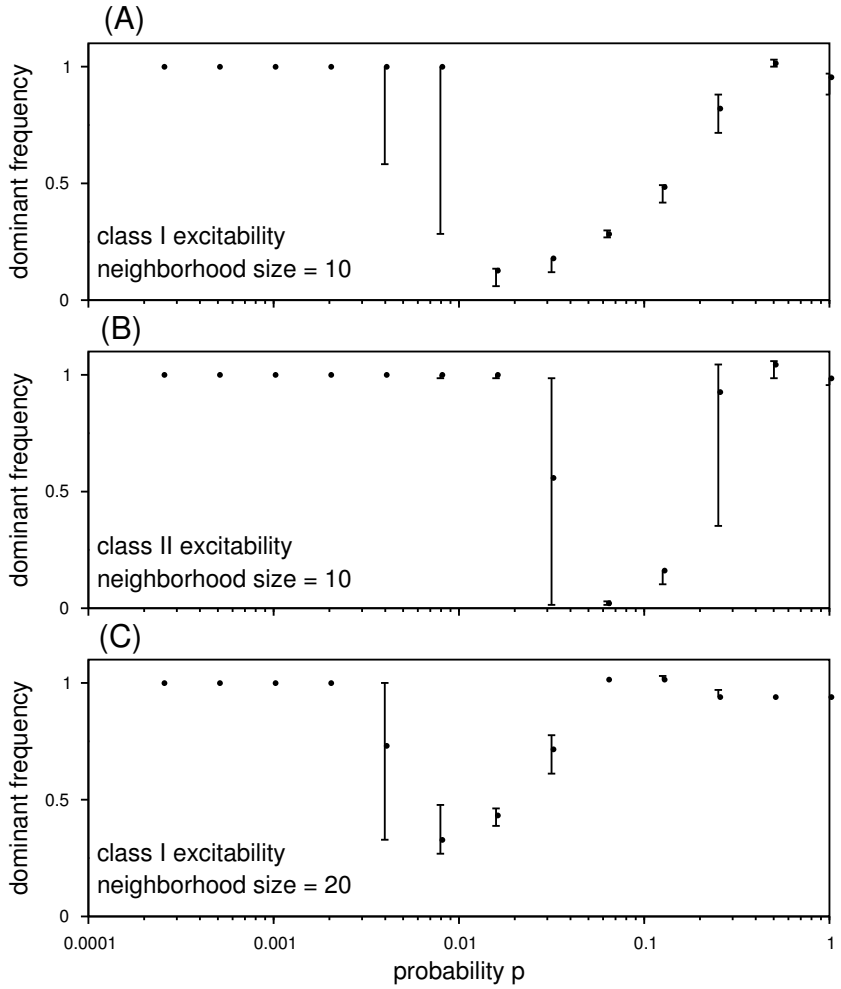


**Figure 15:** *The normalized dominant frequency with the variance in the cellular properties and number of connections in the network.* (A) The normalized dominant frequency of network activity when the component ML cells have class I excitability and the neighborhood size of each neuron is 10. Under this parameter set, bursting activity appears over a broad range of p in the small-world regime. (B) The normalized dominant frequency of network activity when the component ML cells have class II excitability and the neighborhood size of each neuron is 10. (C) The normalized dominant frequency of network activity when the component ML cells have class I excitability and the neighborhood size of each neuron is 20. Under the parameter sets of (B) and (C), bursting activity occurs in the small-world regime but within a narrower range of $p$. The dominant frequency is normalized by the frequency of activity in the regular network (13.4 Hz). The results in (A) and (C) are the medians of 10 random cases with the error bars representing the interquartile range of the 10 random cases. The results in (B) is the median of 4 random cases with the error bars representing the interquartile range of the 4 random cases. The other 6 random cases are not included in calculating the median because the hyperexcited activity are shown in the low $p$ end of the small-world regime in these 6 cases.

assigned to a constant resting potential of $-60$ mV (no current is injected to the resting neurons), rather than having the depolarized or hyperpolarized resting voltage, and these two sets of resting membrane potential result in very similar network activity.

Based on our simulations, small-world bursting robustly emerges regardless of the changes in the properties of the component neurons and the number of connections in the network, although the $p$ range for the bursting appearance shifts in the small-world regime under the variation of certain parameters.

## *3.4 Role of Pacing Neurons in the Generation of Small-world Bursting*

In our simulations, when the pacing neurons are connected to the network, they receive synaptic inputs from other firing neurons. The additional synaptic current increases the firing rate of the pacing neurons during a burst in the small-world regime, as shown in Figure 16(A). To investigate whether the increment in the spiking rate of the pacing neurons was essential for developing a burst and to ascertain whether the feedback connections to the pacing neurons were important for the generation of bursting, we maintained a constant firing frequency by eliminating all the synaptic connections to the pacing neurons. In this case, the pacing neurons unidirectionally drive the network. As shown in Figure 16(B), the network driven by this external periodic input still exhibits bursting activity in the small-world regime, with dynamics similar to those in the network including the pacing neurons. These simulation results suggest that the network bursting is independent of the increment in the spiking rate of the pacing neurons, but a periodic signal, internally or externally generated, is necessary.

To examine the dependence of small-world bursting on the external periodic input, we allowed the pacing neurons to fire limited times, as compared to continuous firing.

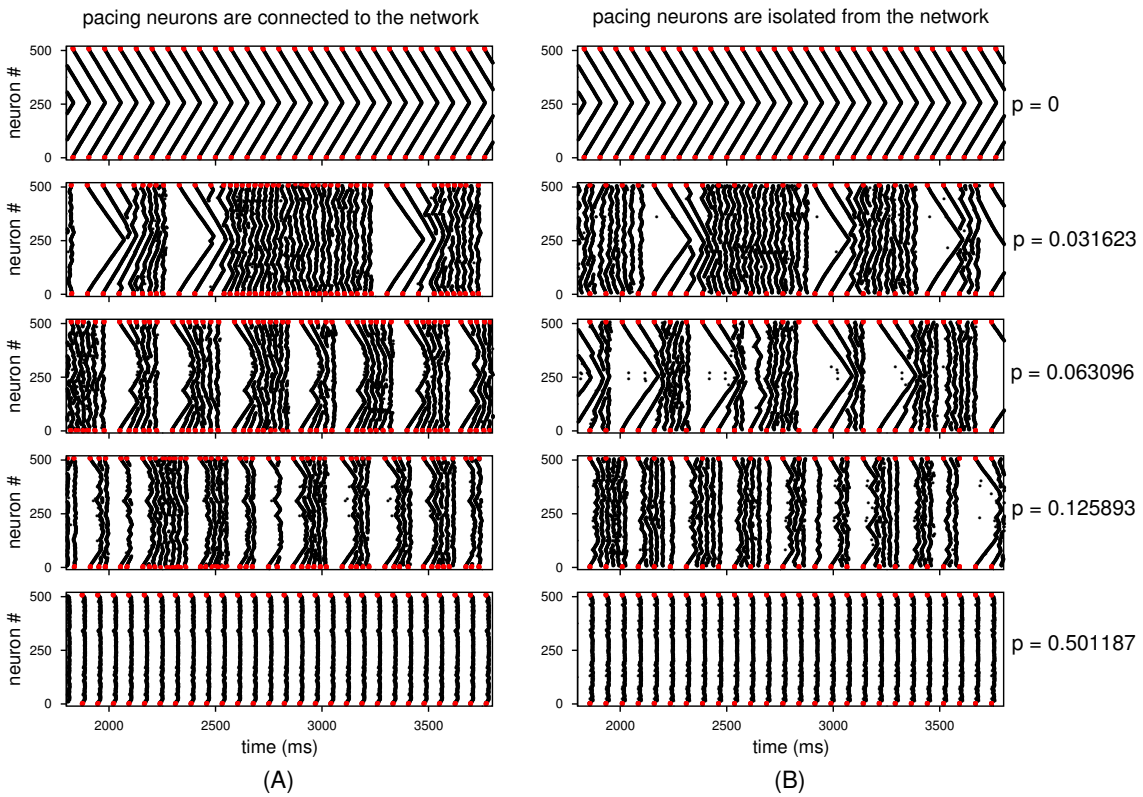


**Figure 16:** *The dynamics of network activity are independent of whether or not the pacing neurons are included in the network.* (A) Raster plots of network activity when the pacing neurons are connected to the network. (B) Raster plots of network activity when the pacing neurons are isolated from the network. The bursting dynamics in the small-world regime, as well as the propagation in the regular network and the tonic beating in the random network, are very similar regardless of the pacing neurons being connected to the network or not.

As shown in Figure 17(A), the pacing neurons fire five times with the same frequency (13.4 Hz) as that of the periodic input in Figure 16(B). After this initial transient input, the network develops a single self-sustained burst. This observation suggests that the rhythmic activity of pacing neurons may initiate a burst but is not necessary for sustaining a burst. Moreover, the spacing between the individual inputs affects the burst initiation and burst duration. As shown in Figure 17(B), if the intervals between the three inputs are large, after transient input ceases, the activity in the network is very low thus a burst can not be initiated. However, when the three spikes in the pacing neurons are close to each other to provide sufficient firing activity in the network, a burst can be evoked. Different spacings between spikes lead the network to different initial states, resulting in bursts with distinct duration, as shown in Figure 17(C)(D).

## *3.5 Enhancement of Small-world Bursting through Network Structure and ML Dynamics*

In the rewiring procedure to construct a small-world network, each connection with probability $p$ is rewired to another neuron chosen uniformly at random over all neurons. Statistically, the long connections in a small-world network obey a uniform random distribution on the ring. To explore whether this small-world network structure supports bursting activity, we gradually altered the uniformity in the random distribution of the long connections. We started with a specific network in which the long connections are uniformly randomly distributed and showed that bursting activity occurs in this network. Then we modified the network structure by constraining those long connections to target cells at a small number of specific regions randomly selected on the ring. As shown in Figure 18, as the number of the local regions decreases, the long connections concentrate more and more to certain locations on the ring. Accompanying with this decreasing uniformity in the distribution

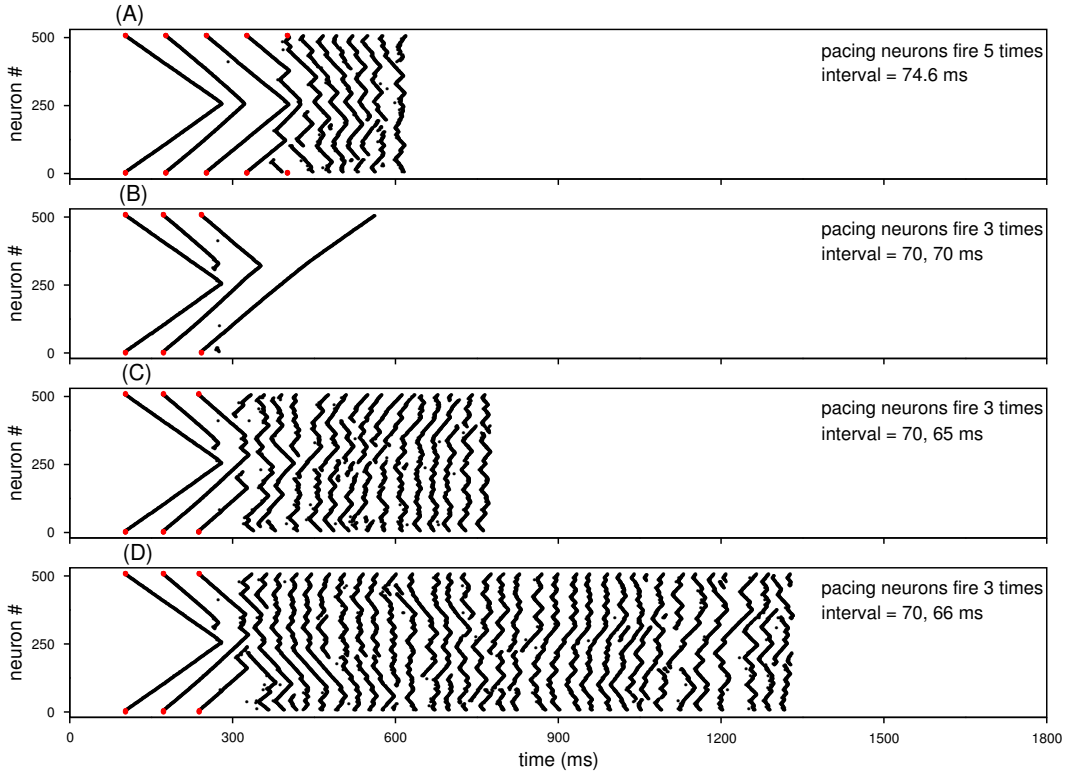


**Figure 17:** *The spacing between inputs affects burst initiation and burst duration.* (A) Raster plot of network activity when the pacing neurons fire five times with the interval 74.6 ms, the same firing frequency as that of the periodic input shown in Figure 16(B). (B) Raster plot of network activity when the pacing neurons fire three times with the intervals 70 ms and 70 ms, respectively. A burst is not initiated. (C) Raster plot of network activity when the pacing neurons fire three times with the intervals 70 ms and 65 ms, respectively. A self-sustained burst is initiated and lasts for approximately 650 ms. (D) Raster plot of network activity when the pacing neurons fire three times with the intervals 70 ms and 66 ms, respectively. A self-sustained burst is initiated and lasts for a significantly longer time than the burst in (C).

of long connections, bursting activity gradually disappears in those networks. This observation suggests that the uniform random distribution of long connections in the small-world networks may be an important feature in the connectivity pattern that supports bursting activity.

In the small-world regime, when the component cells are ML-type neurons, network-wide bursts emerge. However, this small-world bursting can not be reproduced if we replace the ML neurons with Hodgkin-Huxley(HH) or integrate-and-fire(IF) neuron models. This discrepancy between simulation results and our predictions led us to further investigate the differences in ML model and HH model dynamics. As shown in Figure 10, the transient inputs can result in significant voltage deflection in the repolarizing phase of ML action potential. This property is absent in the action potential generated by the HH model. In particular, in terms of the response to the two successive inputs, ML neurons exhibit two unique features. First, the superthreshold duration is extended if a neuron in the superthreshold state receives an input (as shown in Figure 10(B)(D)). Second, a threshold-crossing event can be elicited by a small input after a neuron leaves the superthreshold state (as shown in Figure 10(C)). These two characteristics of ML dynamics may be more reasonably explained by the behavior of bursting neurons, rather than spiking neurons, if the action potential generated by ML equations is treated as the "envelope" of the bursting activity. For example, for a bursting neuron, the activity is often elongated if the neuron receives an input during a burst. This observation may correspond to the extension of the superthreshold duration in the ML model. However, for a spiking neuron, an input is ignored when the neuron remains in the absolute refractory period. Meanwhile, a bursting neuron may produce a short burst if it receives an input at the end of a long burst. This observation is consistent with the property of the ML neuron shown in Figure 10(C). This ML property does not agree with the attributes of a spiking neuron because a small input can not elicit an action potential when the neuron stays

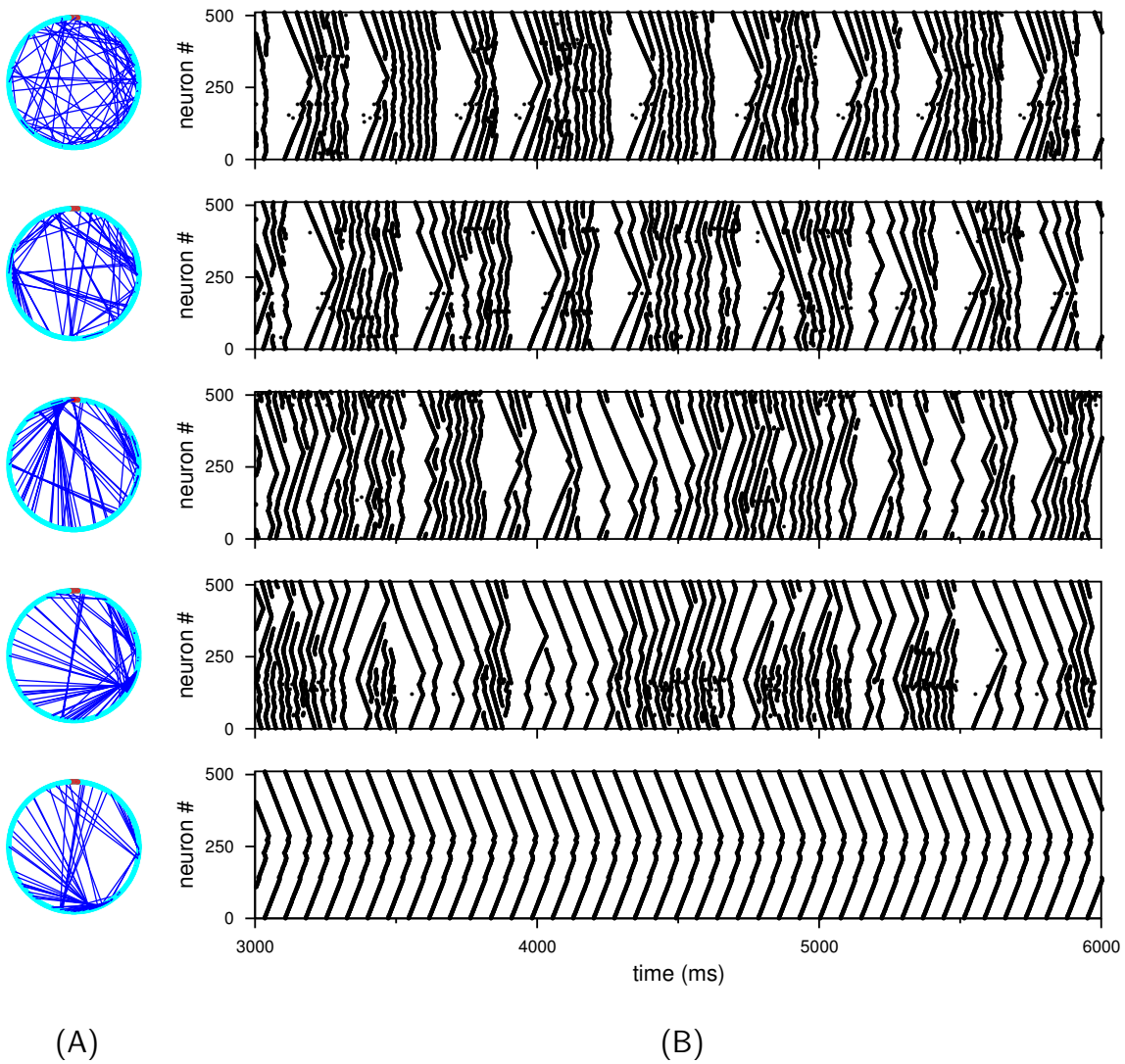


**Figure 18:** *Uniform random distribution of long connections in the small-world network supports bursting activity.* The first ring in column (A) is a small-world network with 77 long connections uniformly randomly distributed on 70 sites on the ring. Bursting activity occurs in this network, as shown in the first raster plot in column (B). From the second to the fifth ring in column (A), the same 77 long connections are rewired to $35, 14, 10$ and 5 positions on the ring, respectively. So the uniformity in the random distribution of long connections gradually decreases. The corresponding raster plots in column (B) (the second to the fifth raster plot) show the bursting activity gradually disappears in the network. The red dots on the top of the rings in column (A) indicate the pacing neurons.

in the relative refractory period.

To clarify whether these distinct dynamics in the ML model facilitate small-world bursting, we proposed a CA model which is similar to an IF model and includes the two features mentioned earlier in the input response of the ML neuron. In order to approximately simulate the relationship between the spiking interval in the pacing neurons of 74.6 ms and the synaptic delay of 1.5 ms in ML model network, we chose 100 time steps as the spiking interval of the pacing neurons and 2 time steps as the synaptic delay in the CA model network. Based on the observation that in the network with ML neurons, the spatial summation of at least three synaptic inputs evokes an action potential, the firing threshold in CA model network is set to 3 with each firing neuron providing a synaptic input of 1. The membrane potential decays with the rate 0.9. The superthreshold duration is about 30 iteration steps if a full action potential is elicited (Figure 10(A)) or 10 iteration steps if a threshold-crossing event is triggered (Figure 10(C)), and this superthreshold duration is extended by 1 iteration step whenever a synaptic input is received by a superthreshold neuron (Figure 10(B)(D)). In the MATLAB programming environment, we implemented the matrix operations and updated the state for each cell in the network based on the set of predefined rules. The network activity converged to stable patterns after the transient died out. The firing activity exhibited in Figure 19 is generated by the same specific network connectivity patterns used in Figure 11 but with the CA model. In Figure 19(A), the CA model includes the two unique input/output features of the ML neuron (described in section 2.2) while in Figure 19(B), those two characteristics are absent in the CA model (in this case, the CA model is roughly equivalent to an IF model).

The comparisons between Figure 11 and Figure 19(A), and between Figure 19(A) and Figure 19(B), show that the CA model is able to reproduce the bursting activity

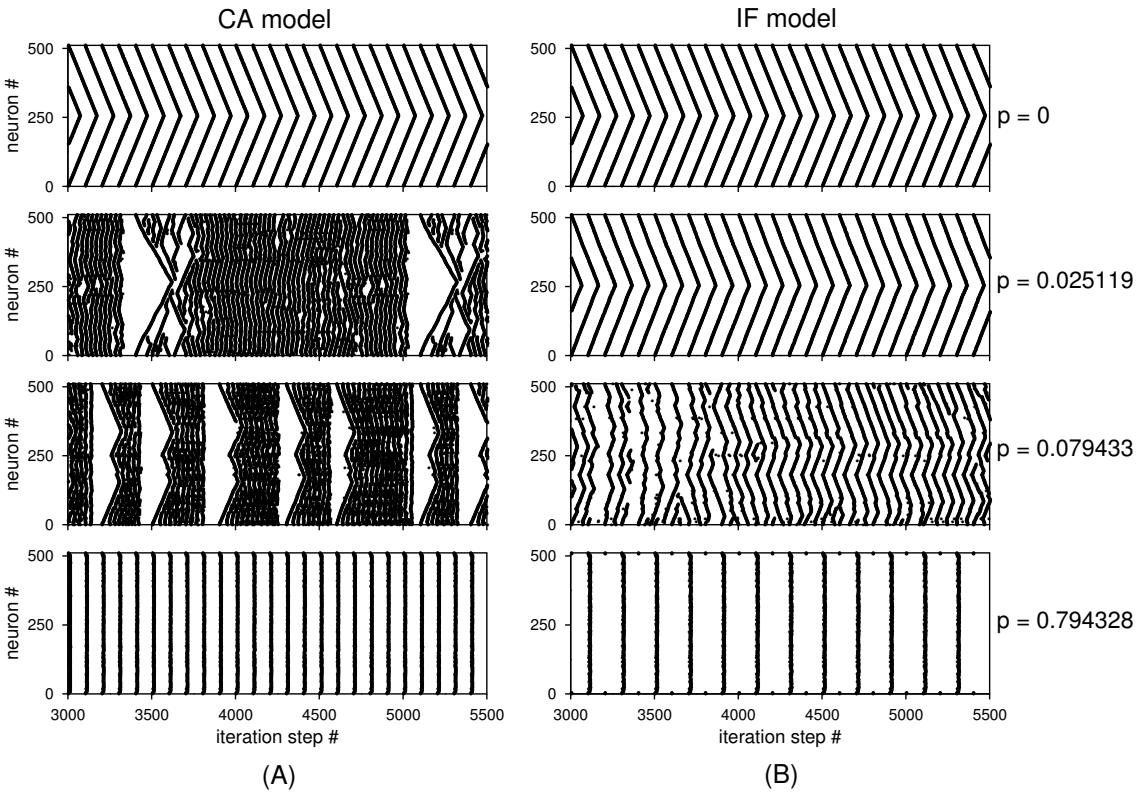


**Figure 19:** *The CA model reproduces the bursting activity generated by ML model in the small-world regime.* (A) Raster plots of the firing activity in the network. The network is constructed by the CA model with the two features in ML dynamics. Bursting activity appears in the small-world regime and it has similar dynamics as that produced by ML model network. (B) Raster plots of the firing activity in the network. The network is constructed by the CA model without the two features in ML dynamics, which is roughly equivalent to a network composed of IF model neurons. This network does not support small-world bursting.

in the small-world regime. In contrast, the CA model without the two salient input/output features of the ML model does not support small-world bursting. These simulation results indicate that the unique dynamics of the component cells, ML model neurons, may foster the bursting activity in the small-world regime.

## *3.6 The Distribution of the Initiating Neurons in the Network*

A burst starts with a long propagation wave, initiated by the pacing neurons which are located at a local region of the network. Due to the long connections, the following propagation waves are gradually initiated by the neurons scattering at different positions on the ring. As the number of initiating neurons increases and the initiating neurons become widely spread in the network, more neurons fire synchronously. To analyze how the distribution of the initiating neurons changes in the network during a burst, we selected eight different bursts with similar durations emerging in the networks with same $p$ value ($p = 0.031623$). For each burst, we found the neurons that initiate a network-wide excitation wave on the raster plot of the network activity, as shown in Figure 20(A). Using a sliding time window of 30 ms, the distance (the number of neurons measured around the ring) between every two adjacent initiating neurons is calculated. The two statistical properties of the distance, the maximum value and the standard deviation, are computed. To establish a comparison standard, we assume that in a time window, the initiating neurons are evenly located on the ring and the distance between every two neighboring initiating neurons is same, that is, $d = 512/$(the number of initiating neurons in that window). The maximum distance, which is called the uniform standard distance (USD), is $d$ and the standard deviation of the distances equals zero. The above calculation was performed on the eight bursts and the median and interquartile range were used to obtain the general trend and the variation in these eight bursts. As shown in Figure 20(B) and (C), statistically,

as a burst develops, the maximum distance between neighboring initiating neurons gradually approaches the USD and the standard deviation of the distances gradually decays to zero. This analysis suggests that during a burst, the positions of initiating neurons gradually approach an even distribution on the ring, which supports the increasing synchronization in the firing time of neurons in the entire network.

In a small-world network with a few long connections, network activity starts with a propagation wave. Due to the existence of sufficient long connections, the new excitation waves are initiated at several positions in the network, increasing the network activity and thus the number of initiating neurons for the following excitation waves. Meanwhile, the uniform random distribution of the long connections facilitates initiating neurons to be evenly distributed in the network. As both the number and the uniformity in the distribution of the initiating neurons gradually increase, network activity progressively achieves synchronization. This synchronization may eventually terminates a burst as most neurons in the network simultaneously enter the refractory state and the network transits to a quiescent phase. Therefore, bursting, characterized by a gradually developed synchronized activity within the burst, appears in the small-world regime.

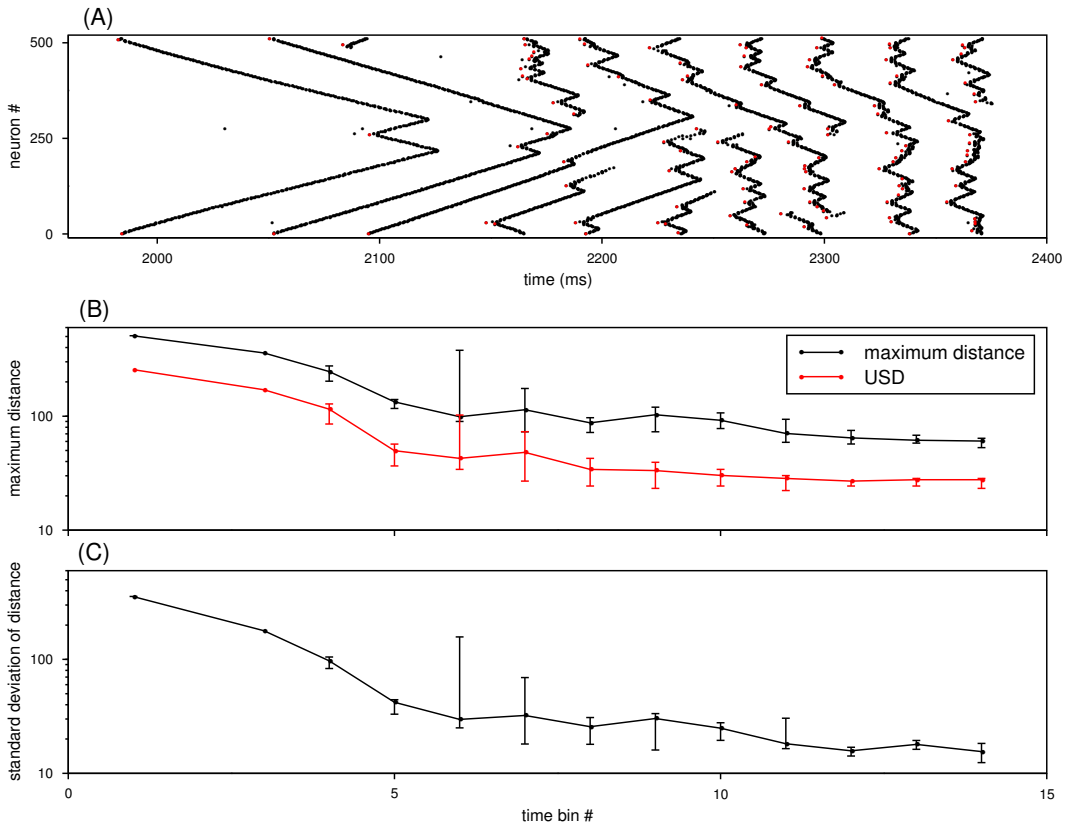


**Figure 20:** *Statistical analysis of the distribution of the initiating neurons in the network during a burst.* (A) Raster plot of the firing activity in the network during a burst. The neurons that initiate the network-wide excitation waves are marked as red dots. (B) The black line is the maximum value of the distance between every two adjacent initiating neurons in a time bin of 30 ms. The red line is the USD (the result is the median of 8 bursts and the error bars represent the interquartile range). At the end of a burst, the USD is approached. (C) Standard deviation of the distances between every two adjacent initiating neurons in a time bin of 30 ms (the result is the median of 8 bursts and the error bars represent the interquartile range). As the burst progresses, the standard deviation decreases.

# CHAPTER IV

# CONCLUSIONS

## *4.1 Summary of Work*

In this thesis, the influence of connectivity topology on network bursting is investigated. Without a slow time-scale process, network-wide bursting activity is observed in a purely excitatory network, when the ML model neurons are coupled in a small-world connectivity pattern. This small-world bursting is robust to changes in cellular properties of the component neurons, initial conditions for the state variables in the ML model, and the number of connections in the network. However, it critically relies on synaptic delays. Further exploration of the mechanism involved in small-world bursting reveals that after a transient input, which provides the network with an initial activity state, a self-sustained burst develops. So the intrinsic properties of the network may play an important role in burst generation. Two inherent attributes of the network are distinguished. First, the uniform random distribution of long connections in a small-world network may support bursting activity because as the uniformity in distribution decreases, network bursts disappear. Second, the unique dynamics of the ML model neuron, in terms of the response to two successive inputs, may facilitate bursting. By utilizing a CA model, two features in ML input/output properties are distinguished and ascertained to be essential for generating bursts. The combination of the uniformly random distributed long connections and ML dynamics enables a burst to start with a long propagation wave and to progressively achieve synchronized firing activity in a small-world network. Although we have not shown it conclusively, the simulation results suggest that the synchronization of the network

activity, which facilitates most neurons in the network enter the refractory state simultaneously, may be a mechanism of burst termination in the absence of an obvious slow process.

## 4.2 Future Work

The simulation results indicate that the network structure (the distribution of long connections) and the dynamics of the component cells (the ML input/output properties) are responsible for the progressively developed synchronization during a burst in a small-world network. However, exactly how these two attributes lead the initiating neurons to gradually become evenly distributed on the ring and thus the network activity from unsynchronized to synchronized firing state has not been discovered, and may need further exploration. Also, for simplicity, in our model network, we assume that distances between each pair of directly connected neurons are the same. However, in biological neural networks, for two connected neurons, the distance can be small if the neurons are adjacent or large if the neurons are far apart. Moreover, the distance between neurons may significantly affect the spatial and temporal summation of the synaptic inputs, determining the generation of an action potential on a postsynaptic neuron, and thus potentially influencing the firing activity of the whole network. The assumption in our model network may be valid if the delay in synaptic transmission is much longer than that is spent on the propagation of an action potential on a neuron axon. For modeling a more realistic neural network, the distance between two connected neurons may be considered and different patterns of network activity may appear.

# APPENDIX A

# MORRIS-LECAR MODEL

The ML model is described by the following two coupled differential equations[15]:

$$
\begin{aligned}
C\frac{dV}{dt} &= -\bar{g}_{Ca}m_{\infty}(V)(V-E_{Ca}) - \bar{g}_{K}w(V-E_{K}) - \bar{g}_{L}(V-E_{L}) + I \\
\frac{dw}{dt} &= \phi\frac{w_{\infty}(V)-w}{\tau_{w}(V)} \\
m_{\infty}(V) &= 0.5(1+tanh(\frac{V-V_{1}}{V_{2}})) \\
w_{\infty}(V) &= 0.5(1+tanh(\frac{V-V_{3}}{V_{4}})) \\
\tau_{w}(V) &= \frac{1}{cosh(\frac{V-V_{3}}{2V_{4}})}
\end{aligned}
$$

where $C$ is membrane capacitance; $V$ is membrane potential; $\bar{g}_{Ca}$, $\bar{g}_{K}$ and $\bar{g}_{L}$ are maximum $Ca^{2+}$, $K^{+}$ and leak conductances, respectively; $E_{Ca}$, $E_{K}$ and $E_{L}$ are reversal potentials of $Ca^{2+}$, $K^{+}$ and leak currents, respectively; $w$ is the fraction of open $K^{+}$ channels; $m_{\infty}$ and $w_{\infty}$ are the fraction of open $Ca^{2+}$ and $K^{+}$ channels at steady state, respectively; $\tau_{w}$ is the time constant for opening of $K^{+}$ channels; $V_{1}$ and $V_{3}$ are half-activation potentials for $m_{\infty}$ and $w_{\infty}$, respectively; $V_{2}$ and $V_{4}$ are the reciprocal of the slopes of the voltage dependence of $m_{\infty}$ and $w_{\infty}$, respectively; $I$ is applied current.

ML neurons possess class I excitability under the parameter set $C = 20\mu F/cm^{2}$, $E_{Ca} = 120mV$, $E_{K} = -84mV$, $E_{L} = -60mV$, $\bar{g}_{K} = 8.0mS/cm^{2}$, $\bar{g}_{L} = 2.0mS/cm^{2}$, $V_{1} = -1.2mV$, $V_{2} = 18mV$, $V_{3} = 12mV$, $V_{4} = 17.4mV$, $\bar{g}_{Ca} = 4.0mS/cm^{2}$ and $\phi = 1/15$, or class II excitability under the same parameter set except $V_{3} = 2mV$, $V_{4} = 30mV$, $\bar{g}_{Ca} = 4.4mS/cm^{2}$ and $\phi = 0.04$.

# APPENDIX B

# CELLULAR AUTOMATON MODEL

*Definition of Parameters*

$N$: the number of neurons in the network

$M$: the firing threshold of a neuron

$k$: the decay rate of the subthreshold potential

$LR$: the large initial value on entering a superthreshold state

$SR$: the small initial value on entering a superthreshold state

$V_{th}$: the threshold for assigning $LR$ or $SR$ to a superthreshold state

$\Delta R$: the amount that the superthreshold duration is extended by any input

*Definition of State Variables*

The three state variables $R, V$ and $F$ are all $N \times 1$ vectors

$R(n)$: an integer variable, superthreshold state at the $n$th iteration step

$V(n)$: a continuous variable, subthreshold state at the $n$th iteration step

$F(n)$: a binary variable, firing state at the $n$th iteration step

Matrix:

$C$: $N \times N$ connectivity matrix

$$C_{ij} = \begin{cases} 1 \quad , \quad if\ neuron\ i\ has\ a\ connection\ to\ neuron\ j \\ 0 \quad , \quad if\ neuron\ i\ does\ not\ have\ a\ connection\ to\ neuron\ j \end{cases}$$

Variable:

$B$: $N \times 1$ input vector, $B_i(n)$ represents the spatial summation of the synaptic inputs received by neuron $i$ at the $n$th iteration step

$nextV$: $N \times 1$ intermediate vector, $nextV_i(n)$ represents the intermediate variable of neuron $i$ at the $n$th iteration step

*Auxiliary Equations*

$$B(n+1) = C \cdot F(n)$$

$$nextV(n+1) = V(n) \times k + B(n+1)$$

*Evolution Equations*

$R_i(n), V_i(n)$ and $F_i(n)$ represent the superthreshold, subthreshold and firing states of neuron $i$ at the $n$th iteration step, respectively.

$$R_i(n+1) = \begin{cases} LR & , \quad if\ F_i(n) = 1\ and\ V_i(n-1) < V_{th} \\ SR & , \quad if\ F_i(n) = 1\ and\ V_i(n-1) \geq V_{th} \\ R_i(n) - 1 + \Delta R & , \quad if\ R_i(n) > 1\ and\ B_i(n+1) > 0 \\ R_i(n) - 1 & , \quad if\ R_i(n) \geq 1\ and\ B_i(n+1) = 0 \\ 0 & , \quad otherwise \end{cases}$$

$$V_i(n+1) = \begin{cases} nextV_i(n+1) & , \quad if\ R_i(n+1) = 0\ and\ nextV_i(n+1) < M \\ M & , \quad otherwise \end{cases}$$

$$F_i(n+1) = \begin{cases} 1 & , \quad if\ R_i(n+1) = 0\ and\ nextV_i(n+1) \geq M \\ 0 & , \quad otherwise \end{cases}$$

The state updating rules in the CA model and their correspondence to the ML dynamics are illustrated in Figure 21. When an action potential is elicited in ML-type neuron i, $F_i$ is set to 1 and lasts for one step. $V_i$ is set to $M$ and maintains $M$ when the neuron is in the superthreshold state. $R_i$ is set to LR in the next step of the firing instant and it decreases 1 in every following step until equals zero. When $R_i = 0$, neuron i is out of the superthreshold state and $V_i$ decays with the rate $k$.

When neuron i receives an input in the superthreshold state, the duration of the superthreshold state is extended by $\Delta R$. $R_i$ is increased by $\Delta R$ instantaneously

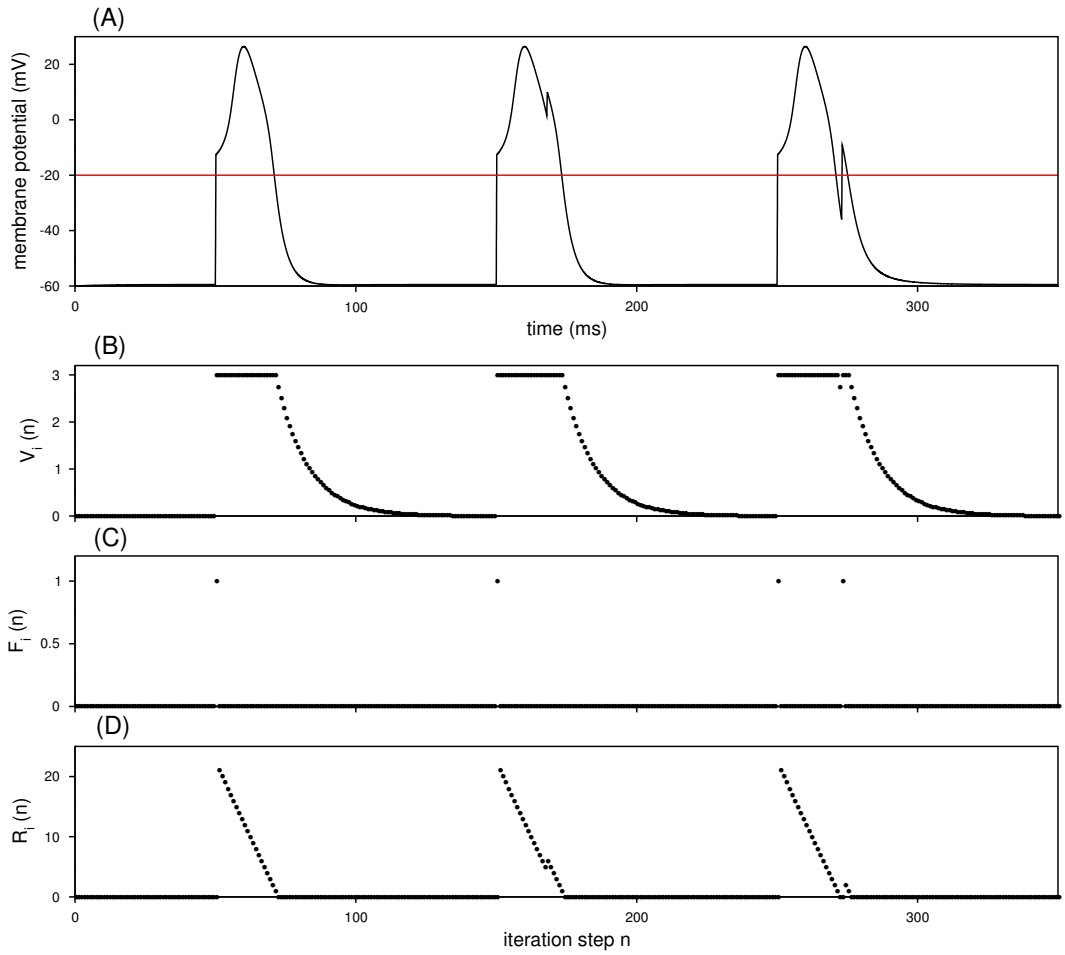


**Figure 21:** *The illustration of the state updating rules in the CA model.* (A) The response of ML-type neuron i to two successive inputs. The red line indicates the firing threshold $-20$ mV. (B) The subthreshold variable for neuron i. (C) The firing variable for neuron i. (D) The superthreshold variable for neuron i.

when the input arrives and then decreases from this increased value. The duration for $V_i = M$ is extended by $\Delta R$.

When neuron i receives an input in the repolarized phase (out of the superthreshold state) and this small input triggers a threshold-crossing event, $F_i = 1$ and $V_i$ is set back to $M$ at the instant of the arrival of the small input. In the next step, $R_i = SR$ since the superthreshold duration for a threshold-crossing event is smaller than the one for an action potential.

# REFERENCES


[1] Agmon-Snir, H., Carr, C. E., and Rinzel, J., "The role of dendrites in auditory coincidence detection," *Nature*, vol. 393, pp. 268–272, 1998.

[2] Bracci, E., Ballerinl, L., and Nistri, A., "Localization of rhythmogenic networks responsible for spontaneous bursts induced by strychnine and bicuculline in the rat isolated spinal cord," *Journal of Neuroscience*, vol. 16, no. 21, pp. 7063–7076, 1996.

[3] Butera, R. J., Rinzel, J., and Smith, J. C., "Models of respiratory rhythm generation in the pre-Bötzinger complex. I. bursting pacemaker neurons," *Journal of Neurophysiology*, vol. 81, pp. 382–397, 1999.

[4] Butera, R. J., Rinzel, J., and Smith, J. C., "Models of respiratory rhythm generation in the pre-Bötzinger complex. II. populations of coupled pacemaker neurons," *Journal of Neurophysiology*, vol. 81, pp. 398–415, 1999.

[5] Del Negro, C. A., Johnson, S. M., Butera, R. J., and Smith, J. C., "Models of respiratory rhythm generation in the pre-Bötzinger complex. III. experimental tests of model predictions," *Journal of Neurophysiology*, vol. 86, pp. 59–74, 2001.

[6] Del Negro, C. A., Morgado-Valle, C., and Feldman, J. L., "Respiratory rhythm: an emergent network property?," *Neuron*, vol. 34, pp. 821–830, 2002.

[7] Endresen, L. P., "Chaos in weakly-coupled pacemaker cells," *Journal of Theoretical Biology*, vol. 184, pp. 41–50, 1997.

[8] Fedirchuk, B., Wenner, P. Whelan, P., Ho, S., Tabak, J., and O'Donovan, M., "Spontaneous network activity transiently depresses synaptic transmission in the embryonic chick spinal cord," *Journal of Neuroscience*, vol. 19, pp. 2102–2112, 1999.

[9] Guare, J., *Six Degrees of Separation:A Play.* New York: Vintage Books, 1990.

[10] Gutkin, B. S. and Ermentrout, G. B., "Dynamics of membrane excitability determine interspike interval variability: a link between spike generation mechanism and cortical spike train statistics," *Neural Computation*, vol. 10, pp. 1047–1065, 1998.

[11] Harris, R. E., Coulombe, M. G., and Feller, M. B., "Dissociated retinal neurons form periodically active synaptic circuits," *Journal of Neurophysiology*, vol. 88, pp. 188–195, 2002.

[12] Hines, M. L. and Carnevale, N. T., "The NEURON simulation environment," *Neural Computation*, vol. 9, pp. 1179–1209, 1997.

[13] Hines, M. L. and Carnevale, N. T., "Expanding NEURON's repertoire of mechanisms with NMODL," *Neural Computation*, vol. 12, pp. 995–1007, 2000.

[14] Montejo, N., Lorenzo, M. N., Perez-Munuzuri, V., and Perez-Villar, V., "Clustering and synchronization in a one-dimensional model for the CA3 region of the hippocampus," *International Journal of Bifurcation and Chaos*, vol. 12, no. 11, pp. 2641–2653, 2002.

[15] Morris, C. and Lecar, H., "Voltage oscillations in the barnacle giant muscle fiber," *Biophysical Journal*, vol. 35, pp. 193–213, 1981.

[16] O'Donovan, M. J., "Motor activity in the isolated spinal cord of the chick embryo: synaptic drive and firing pattern of single motoneurons," *Journal of Neuroscience*, vol. 9, no. 3, pp. 943–958, 1989.

[17] Rekling, J. C. and Feldman, J., "Pre-Bötzinger complex and pacemaker neurons: hypothesized site and kernel for respiratory rhythm generation," *Annu. Rev. Physiol.*, vol. 60, pp. 385–405, 1998.

[18] Rinzel, J. and Ermentrout, B., *Methods in neuronal modeling, Chapter 7: Analysis of neural excitability and oscillation*. MIT Press, 1989.

[19] Skinner, F. K., Kopell, N., and Marder, E., "Mechanisms for oscillation and frequency control in reciprocally inhibitory model neural networks," *Journal of Computational Neuroscience*, vol. 1, pp. 69–87, 1994.

[20] Skinner, F. K. and Mulloney, B., "Intersegmental coordination of limb movements during locomotion: mathematical models predict circuits that drive swimmeret beating," *Journal of Neuroscience*, vol. 18, no. 10, pp. 3831–3842, 1998.

[21] Smith, J. C., Ellenberger, H. H., Ballanyi, K., Richter, D. W., and Feldman, J. L., "Pre-Bötzinger complex: a brainstem region that may generate respiratory rhythm in mammals," *Science*, vol. 254, pp. 726–729, 1991.

[22] Streit, J., "Regular oscillations of synaptic activity in spinal networks in vitro," *Journal of Neurophysiology*, vol. 70, no. 3, pp. 871–878, 1993.

[23] Tabak, J., Senn, W., O'Donovan, M. J., and Rinzel, J., "Modeling of spontaneous activity in developing spinal cord using activity-dependent depression in an excitatory network," *Journal of Neuroscience*, vol. 20, no. 8, pp. 3041–3056, 2000.

[24] Watts, D. J. and Strogatz, S. H., "Collective dynamics of 'small-world' networks," *Nature*, vol. 393, pp. 440–442, 1998.

[25] Wenner, P. Dr. Wenner is a professor in the department of physiology, Emory University School of Medicine. The experiment described in the text is obtained by personal communication with him.

[26] Zhang, L. I. and Poo, M., "Electrical activity and development of neural circuits," *Nature Neuroscience supplement*, vol. 4, pp. 1207–1214, 2001.